BIRDCAGE RESONATOR DESIGN
IN MAGNETIC RESONANCE IMAGING

by

PETER SPRENGER

B.S.E.E
Interkantonales Technikum Rapperswil, Switzerland, 1989

Submitted to the Department of Nuclear Engineering and the Department of
Electrical Engineering and Computer Science
in Partial Fulfillment of the requirements for the Degrees of

Master of Science in Electrical Engineering and Computer Science

and

Master of Science in Nuclear Engineering

Massachusetts Institute of Technology

June 1995

© Peter Sprenger, 1995. All rights reserved
The author hereby grants to MIT permission to reproduce and to
distribute publicly copies of this thesis document in whole or in part

Signature of Author . . . . . .

Certified by . . . . . .
Jerome L. Ackerman, Massachusetts Genearal Hospital
Department of Electrical Engineering and Computer Science
Thesis Advisor

Certified by . . . . . .
Robert M. Weisskoff, Massachusetts General Hospital
Massachusetts General Hospital, Imaging Center
Thesis Advisor

Certified by. . . . . .
David G. Cory, Professor at the Department of Nuclear Engineering
Thesis Reader

Accepted by . . . . . .
Allan F. Henry, Chairman, NED Committe on Graduate Students

Accepted by . . . . . .
F.R. Morgenthaler, Chairman, EECS Committee on Graduate Students

Barker Eng
MASSACHUSETTS INSTITUTE
OF TECHNOLOGY
JUN 07 1995
LIBRARIES

BIRDCAGE RESONATOR DESIGN
IN MAGNETIC RESONANCE IMAGING

by

PETER SPRENGER

Submitted to the Department of Nuclear Engineering and the Department of Electrical Engineering and Computer Science
in Partial Fulfillment of the requirements for the Degrees of
Master of Science in Electrical Engineering and Computer Science and
Master of Science in Nuclear Engineering

ABSTRACT

Circuit equations for the general Birdcage resonator are solved with a polynomial approach and an expression for the resonant frequencies is derived. The results are compared with numerical calculations and with experiments on a 12 mesh, low pass Birdcage. A design procedure for low pass Birdcages, which follows directly from the polynomial analysis, is presented. It is shown that the resonant frequencies can be divided into low and high impedance resonant modes and that the total number of resonant frequencies is equal to the number of meshes. The angular current distribution in the legs of the resonator is derived using the polynomial approach. Two methods of measuring the currents in the legs of the resonator are proposed and verified experimentally.
A resonator tuned to its second mode can be viewed as a surface coil wrapped around the sample and thus yields an increased Signal to Noise ratio at the edge of the resonator. This increase is calculated theoretically for a spherical sample and the experimental value is in good agreement.
A description of the transmission line is included since the concept is useful for the understanding of the Birdcage resonator.

Thesis Supervisor for NED: Dr. Robert M. Weisskoff

Thesis Supervisor for EE: Dr. Jerome L. Ackerman

Table of contents

1.	**Introduction**	
1.1	Thesis description	7
1.2	The MR experiment	8
2.	**Coil design**	
2.1	Introduction	11
2.2	Transmission Lines	12
2.3	Matching of MR coils	28
3.	**Birdcage resonator**	
3.1	Motivation	32
3.2	Principle of the Birdcage Resonator	35
3.3	Resonance frequencies	38
3.4	Current distribution	52
3.5	Numerical Methods	58
3.6	RF Field distributon	67
3.7	SNR considerations	72
3.8	Experimential results	76
4.	**Practical consideration**	
4.1	Adjustment of Birdcage	87
5.	**References**	101
6.	**Conclusions**	102
7.	**Final remarks / Acknowledgements**	103
	Appendix	
	A	105
	B	112
	C	115
	D	116
	E	120
	F	123

1. Introduction

1.1 Thesis description

Magnetic resonance imaging (MRI) is one of various mapping modalities that have been applied for the creation of images. The most important application is its use as a medical diagnostic tool. One of the main advantages of MRI over conventional CT (X-ray) tomography are the relatively low photon energies, in the order of 10^{-7} eV, compared to 10-1000keV used in CT's [1]. This advantage however results in a much weaker received signal. Several experimental techniques can be applied to enhance the sensitivity of an MR image. In particular, if the object does not change in time, the MR experiment can be repeated and the collected information averaged yields an enhanced signal to noise ratio. In medical diagnostics however imaging time is limited and patients cannot be assumed to be rigid objects.

A particular important piece of the MRI scanner hardware is the sensor which picks up the electro magnetic radiation, produced by the magnetic moments of the nuclei inside the object. Several types of different sensors (in fact these are wire loops called coils) are used in MRI, depending on the object to be imaged and the type of experiment used. A particular design of such a coil is subject of this thesis. It provides an increased sensitivity over a limited spatial section. Since this sensor is intended to be used for functional MRI, the region of interest is the cortex of the human brain. Surface coils have previously been used to pick up the signal at a specific spatial point. The approach used here, is a special design of a Birdcage resonator [2], tuned to a resonance mode which covers a spatial area close to the one of the human cortex.

The thesis introduces the basic concepts of coil design in NMR (chapter 2) and presents a new way of predicting the resonance frequencies of Birdcage resonators and compares the results with existing theories [2,3] (chapter 3.3 .. 3.5) The improved sensitivity of a Birdcage tuned to the second mode (gradient Birdcage) is shown (chapter 3.7). Theoretical predictions are compared with experiments. (chapter 3.8) A useful tool to adjust Birdcage resonators is presented in chapter 4.

1.2 The MR experiment

In order to understand the objective of this thesis, it is useful to first summarize the NMR experiment [4,5].

Consider a system at the microscopic level characterized by the quantum mechanical angular momentum $L = j\hbar$, where j is the angular momentum quantum number, and h is Planck's constant. The absolute value squared of the angular momentum is given by

EQ1

$$L^2 = [j(j+1)]\hbar^2.$$

A particle with angular momentum has a magnetic dipole moment whose magnitude is given by

EQ2

$$\mu = \gamma h\bar{}\sqrt{j(j+1)} \ ,$$

where γ is the magnetogyric ratio. The energy of the magnetic moment μ in the presence of a static magnetic field H is,

EQ3

$$E = -\mu \cdot H = -\mu H \cos\theta \ ,$$

where θ is the angle between the magnetic moment and the magnetic field. Classically, a magnetic moment can assume any orientation with respect to the magnetic field i.e. θ can have any value from 0 to π. However, quantum mechanics restricts the number of such orientations such that the projection of μ upon the magnetic field direction is limited to a finite set of values. Its projection upon the magnetic field is $\gamma m\hbar$, where m is restricted to the following,

EQ4

$$m = j, (j-1), (j-2), ..., -(j-2), -(j-1), -j \ .$$

The proton has an intrinsic angular momentum (spin) of S=1/2. The magnetic moment associated with spin is given by,

EQ5

$$|\mu| = \gamma h\bar{}\sqrt{S(S+1)} \ .$$

For the proton, γ is 265.5×10^6 rad $s^{-1}T^{-1}$. Thus a proton in a magnetic field has only two allowed states (i.e. +/- 1/2). The energy separation between these states are given by,

EQ6

$$\Delta E = \gamma \hbar H \ .$$

The linear dependence of the Energy difference is shown in Fig. 1:

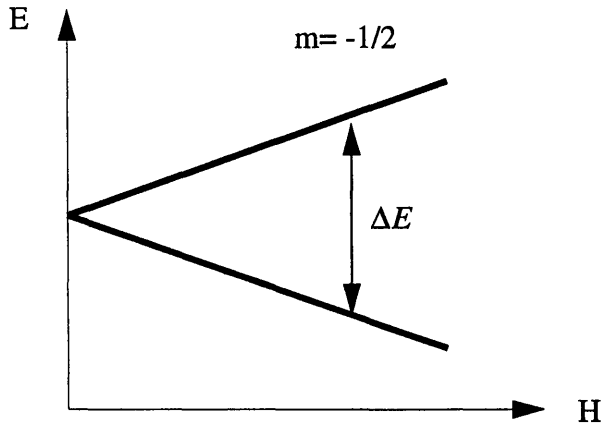

Fig.1: energy difference as a function of magnetic field

Classically, the change of angular momentum over time (i.e. dL/dt) is equal to the applied torque $\vec{\tau} = \vec{\mu} \times \vec{H}$. Hence, a magnetic dipole moment in a magnetic field will experience a time rate of change of angular momentum. From EQ1 and EQ2 we know that

EQ7

$$\mu = \gamma L \ ,$$

and thus we can write:

EQ8

$$\frac{d}{dt}\vec{\mu} = \gamma(\vec{\mu} \times \vec{H}) .$$

Since the torque acting on a system is perpendicular to both $\vec{\mu}$ and $\vec{H}$, the resulting motion will be a precession of $\vec{\mu}$ about the magnetic field. Let z be the direction of the magnetic field and M_x, M_y and M_z be the components of $\vec{\mu}$. Now suppose a radiation field of frequency $\omega_0 = \gamma H_0$ is impressed upon a system of protons having an x-component whose time dependence is $H_x = H_x^0 \cos(\omega_0 t)$. Such a linearly polarized field may be expressed as the sum of two counter-rotating circularly polarized fields H_l and H_r, where H_r is

a field that rotates about the z-axis in a counter clockwise manner, while H_1 rotates about the z-axis clockwise. The only component of H_x that affects the magnetization vector is H_r, which rotates in the same sense as does the precession of the magnetization vector. In the rotating frame, H_r remains in phase with M imparting a constant torque upon the latter. This torque causes M to undergo a continuous increase in its polar angle θ. The increase in θ will continue as long as the system is exposed to the oscillating field H. The angular motion of M is called nutation. Clearly the nutation frequency depends linearly on the strength of the of the oscillating field H.

Suppose the oscillating field H is applied for a period of $\pi/2\omega_0$ then the magnetization M will be aligned parallel to the y axis. This is not a state of thermal equilibrium; hence the system will move towards thermal equilibrium. During this time the oscillating magnetization will induce an EMF in the antenna which previously generated the oscillating field H.

A special antenna (called Birdcage resonator) which creates the field H and receives the magnetization M is subject of this thesis. An improved antenna design will affect both, the nutation frequency and the intensity of the induced EMF [6].

2. Coil design

2.1 Introduction

The purpose of an NMR coil is to create a magnetic RF field to perturb the spin system. Therefore the design is focused on the optimization of the mag-

netic field produced by the coil. The photon energy is proportional to the static magnetic field B_0 and is in the order of 0.5eV which corresponds to a frequency of approx. 100MHz (see 1.2). This frequency range is heavily used by broadcasting stations, telecommunications etc. and thus a well investigated field of engineering is available to the coil designer. In fact we will use basic knowledge in radio engineering i.e. impedance matching, resonance networks, transmission lines etc. to develop a new coil design. An ideal NMR coil has the following characteristic:

a) magnetic field intensity and phase is the same at any point in space

b) no heating of the coil (i.e. no resistive losses)

c) no power break down

d) no electrical field within the subject

In practice none of these ideal characteristics can be met. The optimization of a particular characteristic has to be compromised by a decreased performance of another aspect. For this reason many different coil designs are used. In this work we concentrate on the optimization of the sensitivity in a particular region of interest. First however we want to introduce a few basics in the world of coil design.

2.2 Transmission Lines

Transmission lines in the coil design for NMR have a two fold significance. First they deliver the electromagnetic energy from the radiation source (i.e. the RF amplifier) to the coil and the small signal received by the coil (i.e. the NMR signal) to the RF receiver. To have an optimum energy transfer, the

devices (coils, receivers transmitters etc.) inter connected with transmission lines have to be matched. In chapter 2.3 we will explore the concept of matching. Second, transmission lines can be used as models to gain a better understanding of special NMR coils (i.e. Birdcage resonators). Here the concept of transmission lines is introduced as it is applicable to the design of NMR coils.

2.2.1 Overview

According to the electromagnetic model [11], time varying charges and currents are sources of electromagnetic fields and waves. The waves carry electromagnetic power and propagate in the surrounding media with the velocity of light (in vacuum). In open space power transmission is very inefficient. Even when a source radiates with the aid of highly directive antennas, its power spreads over wide range and thus resulting in a low power density. For an efficient point to point transmission of power, the source energy must be guided. Here we consider the transmission of transverse electromagnetic waves (TEM) in coaxial transmission lines, since this is most commonly used in NMR.

The general transmission-line equation can be derived from a circuit model in terms of resistance, inductance, conductance and capacitance per unit length of the line. From these equations, all the characteristics of wave propagation along a given line can be derived and studied. The investigation of time-harmonic steady state properties of transmission lines are facilitated by the use of graphical charts, which eases the necessity of repeated calculations with complex numbers. The best known and most widely used graphical chart is the Smith Chart.

2.2.2 General transmission line equations

Consider a uniform transmission line consisting of two parallel perfect

conductors. The distance of separation between them is small in comparison with the operating wavelength. Since ordinary electric networks have physical dimensions much smaller than the operating wavelength, they can be represented by lumped parameters. The voltage between the conductors and the currents along the line are closely related to the transverse components of the electric and magnetic field. We find that the dependence of these field components on the transverse coordinates is the same as under static conditions. Thus the parameters of a transmission line can be determined by methods used under static conditions. Transmission lines differ from ordinary electric circuits in one important feature. The physical dimensions of electric networks are very much smaller than operating wavelength whereas transmission lines are usually longer than the operating wavelength and may even be several wavelengths long. In lumped element circuits it is assumed that there are no reflection and standing waves. Therefore a lumped parameter model of the transmission line can only be valid if the line is much shorter than the operating wavelength. This leads to the concept of distributed circuits parameters throughout the entire length of the transmission line and lumped element parameters are given for a differential length dz. Consider a transmission line with length dz and the following parameters:

-R, resistance per unit length [Ω/m]

-L, inductance per unit length [Vs/Am]

-G, conductance per unit length [Ω^{-1} /m]

-C, capacitance per unit length [As/Vm]

Then we can draw the equivalent lumped electric circuit for the length dz:
The quantities v(z,t) and v(z+dz,t) denote the instant voltages at position z and z+dz and i(z,t), i(z+dz,t) the currents at z and z+dz along the transmission line. We can apply Kirchoff's voltage law,

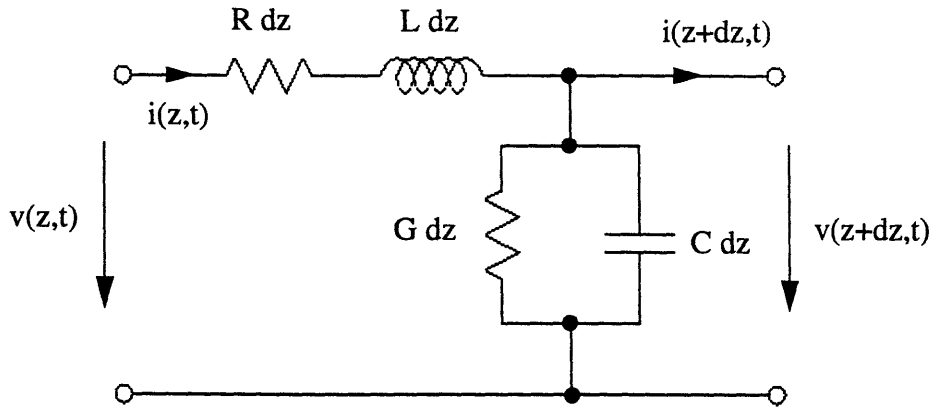

Fig.2: Transmission line equivalent circuit

EQ9

$$-\frac{v(z+dz,t)-v(z,t)}{dz} = Ri(z,t) + L\frac{\partial}{\partial t}i(z,t) \quad .$$

Similarly we apply Kirchoffs current law,

EQ10

$$-\frac{i(z+dz,t)-i(z,t)}{dz} = Gv(z+dz,t) + C\frac{\partial}{\partial t}v(z+dz,t) \quad .$$

As dz approaches zero EQ 9 and EQ 10 reduce to,

EQ11

$$-\frac{\partial}{\partial z}v(z,t) = Ri(z,t) + L\frac{\partial}{\partial t}i(z,t) \quad ,$$

EQ12

$$\frac{\partial}{\partial z}i(z,t) = Gv(z,t) + C\frac{\partial}{\partial t}v(z,t) \quad .$$

EQ11 and EQ12 are the general transmission line equations. Since here we are primarily interested in harmonic time dependence, we can rewrite EQ11 and EQ12,

EQ13

$$-\frac{\partial}{\partial z}V(z) = (R+j\omega L)\,I(z) \quad ,$$

EQ14

$$-\frac{\partial}{\partial z}I(z) = (G+j\omega C)\,V(z) \quad ,$$

where ω is the frequency of the sinusoidal signal. EQ13 and EQ14 are linear and thus no harmonics can occur. Note that the current and the voltage are function of the spatial coordinate (i.e. z) only. Extracting V(z) from EQ 14 and substituting into EQ13 and similarly solving for I(z) in EQ13 and substituting into EQ14 yields the time harmonic transmission line equations,

EQ15

$$\frac{d^2}{dz^2}V(z) = \gamma^2 V(z) \quad ,$$

EQ16

$$\frac{d^2}{dz^2}I(z) = \gamma^2 I(z) \quad ,$$

where γ is a complex number called the propagation constant:

EQ17

$$\gamma = \sqrt{(R+j\omega L)\,(G+j\omega C)} = \alpha + j\beta \quad .$$

We can clearly see that the transmission line is completely defined by its distributed parameters R,L,G,C. In general, these quantities depend on ω in a complicated way. However we will assume that these transmission line parameters depend only on the physical dimensions of the transmission line.

2.2.3 Coaxial transmission line parameters

As we have seen, the knowledge of R,L,G,C allows us to completely characterize the transmission line. A coaxial cable consists of an inner conductor and an outer conducting shield separated by a dielectric medium. This structure has the important advantage of confining the electric and magnetic fields entirely within the dielectric region and little external interference is coupled into the line. Most NMR instruments use coaxial cable as wave guides since they are very easy to handle and the cable losses (represented by R and G) are reasonably small. A cross section of the line is shown in the figure below.

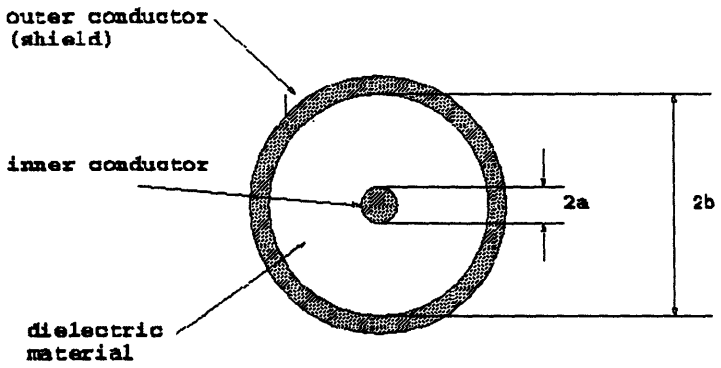

Fig.3: Cross section of a coaxial transmission line

The transmission line parameters are,

EQ18

$$R = \frac{1}{2\pi}\left(\frac{1}{a}+\frac{1}{b}\right)\sqrt{\frac{\pi f \mu_c}{\sigma_c}} \quad [\Omega/m\,]$$

EQ19

$$C = \frac{2\pi\varepsilon}{\log(b/a)} \quad [\mathrm{F/m}]$$

EQ20

$$L = \frac{\mu}{2\pi}\log\frac{b}{a} \quad [\mathrm{H/m}]$$

EQ21

$$G = \frac{2\pi\sigma}{\log(a/b)} \qquad [\mathrm{S/m}]$$

where σ is the conductivity, μ the permeability, ε the dielectric constant of the material between the inner conductor and the shield. μ_c and σ_c represent the permeability and the conductivity of the conductor material. Note that in EQ18 the square root term is the real part of the intrinsic impedance which is related to the skin effect. For our purposes we can set R=0 since the conductivity of the conductors in a transmission line is high and the frequency low (order 100MHz) that the effect of R on the computation of the propagation constant is negligible.

2.2.4 Wave characteristics of an infinitely long transmission line

From EQ15 and EQ16 we know the time harmonic spatial functions I(z) and V(z) along the transmission line. Solving these equations yields

EQ22

$$V(z) = V_{tl}e^{-\gamma z} + V_{ts}e^{\gamma z} \quad ,$$

EQ23

$$I(z) = I_{tl}e^{-\gamma z} + I_{ts}e^{\gamma z} \quad ,$$

where the indices *tl* and *ts* denote a wave traveling toward the load (i.e. in +z direction) and toward the source (i.e. in -z direction). Assuming the case of an infinitely long cable we do not expect a wave traveling in the -z direction. Thus we can neglect the right terms in EQ22 and EQ23. The impedance at the input of the infinitely long transmission line is V(z)/I(z). Substituting EQ22and EQ23 into EQ13 yields

EQ24

$$Z_0 = \frac{V(z)}{I(z)} = \frac{(R+j\omega)}{\gamma} = \sqrt{\frac{R+j\omega L}{G+j\omega C}} \ .$$

Neglecting the resistive parts in EQ24, the characteristic impedance Z_0 is $\sqrt{L/C}$ and does not depend on the frequency. Note that Z_0 is a characteristic property of the transmission line whether the cable is infinitely long or not. An infinitely long lin simply implies that there are no reflected waves and thus its input impedance is Z_0. The phase velocity in the lossless transmission line is ω/β and thus with EQ17 $(LC)^{-1/2}$.

2.2.5 Wave characteristic of the finite transmission line

Using EQ22 and EQ23 again and substituting I(z) and V(z) into EQ13 and EQ14 we can see that,

EQ25

$$\frac{V_{tl}}{I_{tl}} = -\frac{V_{ts}}{I_{ts}} = Z_0 \ .$$

Now consider a finite length transmission line with an arbitrary chosen impedance Z_l at the end of the line (i.e. z=l) and a sinusoidal voltage source V_0 at the input of the transmission line.(i.e z=0) as depicted in the following Fig.4.

As suggested above Z_0 is a property of the transmission line and depends only on the physical dimensions. Z_l is any complex impedance. EQ22 and EQ23 must be satisfied at all positions and in particular at z=l and z=0. First let z=l and solve EQ25 for V_{tl} and V_{ts}.

EQ26

$$V_{tl} = \frac{I_l}{2}(Z_l + Z_0)\, e^{\gamma l} \ ,$$

EQ27

$$V_{ts} = \frac{I_l}{2}(Z_l - Z_0)\, e^{-\gamma l} \quad .$$

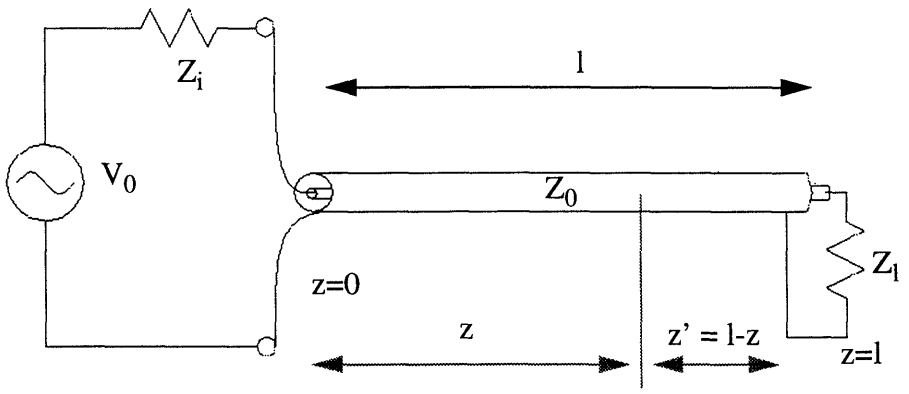

Fig.4: Finite length transmission line with complex impedance Z_l

Substituting EQ26 and EQ27 into EQ22 and EQ23 yields,

EQ28

$$V(z) = \frac{I_l}{2}[\,(Z_l + Z_0)\, e^{\gamma(l-z)} + (Z_l - Z_0)\, e^{-\gamma(l-z)}\,] \quad ,$$

EQ29

$$I(z) = \frac{I_l}{2Z_0}[\,(Z_l + Z_0)\, e^{\gamma(l-z)} - (Z_l - Z_0)\, e^{-\gamma(l-z)}\,] \quad .$$

With help of the figure above we can substitute l-z with z' and using the hyperbolic functions sinh ($\gamma z'$) and cosh ($\gamma z'$) we can write EQ28 and EQ29 in the simpler form,

EQ30

$$V(z') = I_l(Z_l \cosh\gamma z' + Z_0 \sinh\gamma z') \quad ,$$

EQ31

$$I(z') = \frac{I_l}{Z_0}(Z_l \sinh\gamma z' + Z_0 \cosh\gamma z') \quad .$$

EQ30 and EQ31 can be used to find the current and the voltage at any point

along the transmission line in terms of Z_l,Z_0,I_l and γ . With the impedance at any point along the line being $Z(z') = V(z')/I(z')$ EQ30 and EQ31 reduce to,

EQ32

$$Z(z') = Z_0 \frac{Z_l + Z_0 \tanh \gamma z'}{Z_0 + Z_l \tanh \gamma z'} \quad .$$

At the source z=0, z' is l and thus the input impedance is,

EQ33

$$Z_{in} = Z(l) = Z_0 \frac{Z_l + Z_0 \tanh \gamma l}{Z_0 + Z_l \tanh \gamma l} \quad .$$

Since the generator "sees" the input impedance Z_{in} we could replace the transmission line and the load Z_l with the impedance Z_{in}. From the above equations it is also clear, that for Z_l=Z_0 the input impedance will always be Z_0 no matter how long the transmission line is. With EQ27 we find that V_{ts} (i.e. the magnitude of the reflected wave) is 0 for the Z_l=Z_0 case.

2.2.6 Standing waves and reflections on transmission lines

From above discussion we know that there is reflection atZ_l if different from Z_0. The reflection coefficient is a convenient measure of the amount of reflection. It is simply the ratio between voltage traveling towards the source (i.e. reflected from the load) and the voltage traveling towards the load. With $V_{tl}(z) = V_{tl}e^{-\gamma z}$ (i.e the wave traveling towards the load) and $V_{ts}(z) = V_{ts}e^{\gamma z}$ we can take the ratio to yield the (in general complex) reflection coefficient,

EQ34

$$\Gamma(z) = \frac{V_{ts}}{V_{tl}} e^{2\gamma z} \quad .$$

To calculate the reflection at the load Z_l we can substitute EQ26 and EQ27 into EQ34,

EQ35

$$\Gamma = \frac{Z_l - Z_0}{Z_l + Z_0} \quad .$$

Note that the voltage reflection coefficient is measured at the load which is connected to the voltage source with a transmission line of length l. With EQ25, we find the current reflection coefficient to be the negative of the voltage reflection coefficient. From EQ35 we can also see that the load impedance Z_l is directly related to the amount of reflection occurring at z=l. This allows an indirect measurement of complex impedances. The bilinear transformation in EQ35 is the basis of a widely used graphical chart (i.e. the Smith-Chart) to perform otherwise tedious complex calculations.

2.2.7 The Smith Chart

In general the reflection factor defined in EQ35 is a complex number that is written as,

EQ36

$$\Gamma = \frac{Z_l - Z_0}{Z_l + Z_0} = |\Gamma| e^{j\angle\Gamma} \quad .$$

Dividing denominator and nominator of EQ36 by Z_0 results in

EQ37

$$\Gamma = \frac{z_l - 1}{z_l + 1} = |\Gamma| e^{j\angle\Gamma} \quad ,$$

where $z_l = Z_l / Z_0$ is the normalized impedance.

Solving EQ37 for z_l yields

EQ38

$$z_l = \frac{1+\Gamma}{1-\Gamma} \quad .$$

With $z_l = r + jx$ and $\Gamma = \Gamma_r + j\Gamma_i$ substituted into EQ38 yields

EQ39

$$r + jx = \frac{1+\Gamma_r + j\Gamma_i}{1-\Gamma_r - j\Gamma_i} \quad .$$

Multiplication of the numerator and denominator of EQ39 with its complex conjugate yields separated real and imaginary parts. Thus we can write

EQ40

$$r = \frac{1-\Gamma_r^2-\Gamma_i^2}{(1-\Gamma_r)^2+\Gamma_i^2} \quad ,$$

and

EQ41

$$x = \frac{2\Gamma_i}{(1-\Gamma_r)^2+\Gamma_i^2} \quad .$$

If we vary the imaginary part of the normalized impedance z_l (i.e. x) and keep its real part r fixed, the bilinear transformation of EQ37 yields a circle in the complex reflection plane. To see this, we rewrite EQ40

EQ42

$$\frac{1-r}{1+r} = \Gamma_r^2 - 2\frac{r\Gamma_r}{1+r} + \Gamma_i^2 \quad .$$

Adding $r^2/(1+r)^2$ on each side yields

EQ43

$$\left(\frac{1}{1+r}\right)^2 = \left(\Gamma_r - \frac{r}{1+r}\right)^2 + \Gamma_i^2 \quad ,$$

which can be recognized as a circle with its center at $\{r/(1+r), 0\}$ and radius $1/(1+r)$.

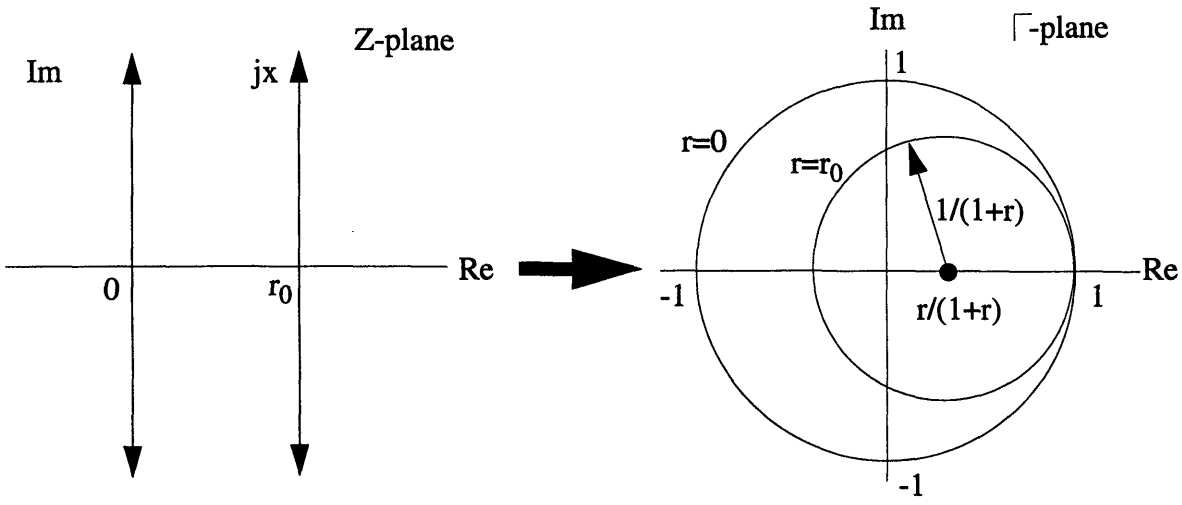

Fig.5: Mapping of impedance with varying imaginary part to the reflection plane

Similarly we rewrite EQ41 to yield

EQ44

$$\left(\frac{1}{x}\right)^2 = (\Gamma_r - 1)^2 + \left(\Gamma_i - \frac{1}{x}\right)^2 \quad .$$

Thus varying the real part of the normalized impedance z_l yields a circle with

its center at $\{1, 1/x\}$ and radius $1/x$. Fig.6 depicts this transformation

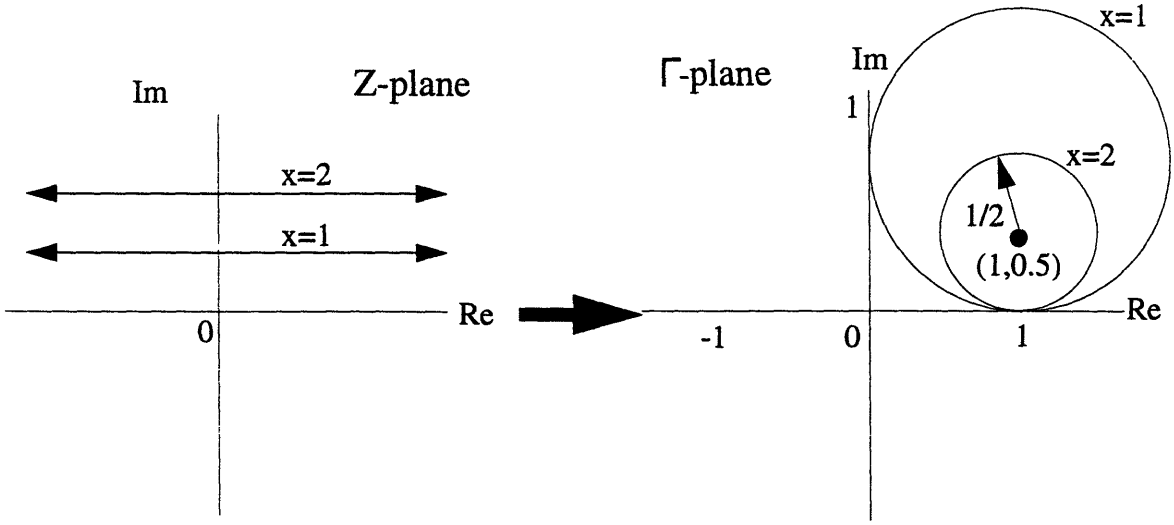

Fig.6: Mapping of impedance with varying imaginary part to the reflection plane

The Smith chart is a collection of several above derived circles.

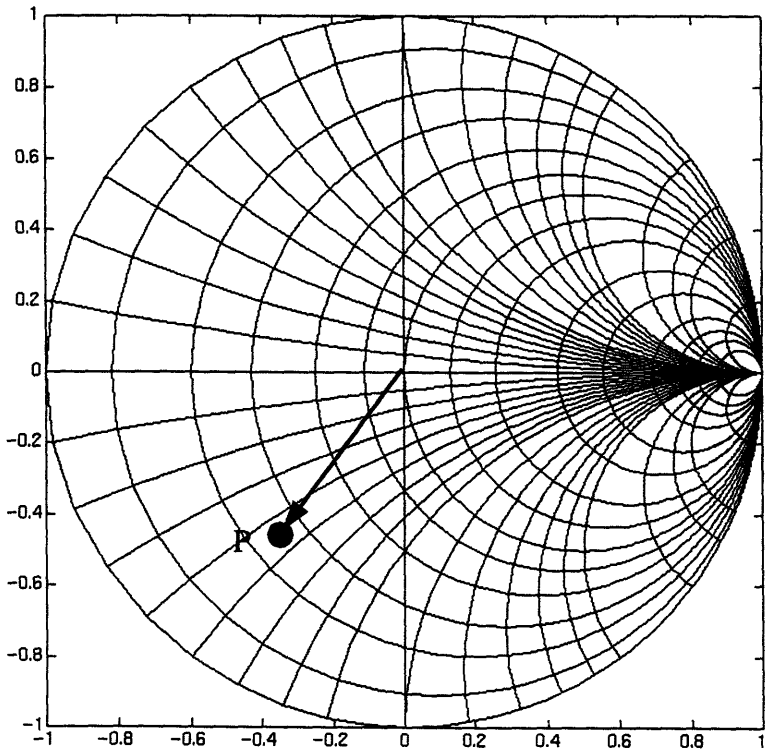

Fig.7 Impedance Smith Chart

Notice that any point P positioned on the Smith chart represents a unique impedance that can be determined by EQ38 and the characteristic transmission line impedance Z_0 (undo of normalization).

In many cases it is helpful to look at the transformation of the reciprocal value of the impedance to the reflection factor (i.e. admittance <=> reflection transformation).

Let Γ_z be the complex reflection of the impedance z and Γ_b be the complex reflection of the admittance $b = 1/z$. Using EQ37 we can write:

EQ45

$$\Gamma_b = \frac{1/z - 1}{1/z + 1} \ .$$

Multiplying denominator and numerator by z yields

EQ46

$$\Gamma_b = -\frac{z-1}{z+1} = -\Gamma_z \ .$$

Thus the reciprocal operation applied to an impedance corresponds to a angular rotation operation of π in the reflection plane. This relation is particularly useful when dealing with parallel impedances and transmission lines. Performing this transformation on the impedance Smith chart of Fig.7 yields the admittance Smith chart of Fig.8

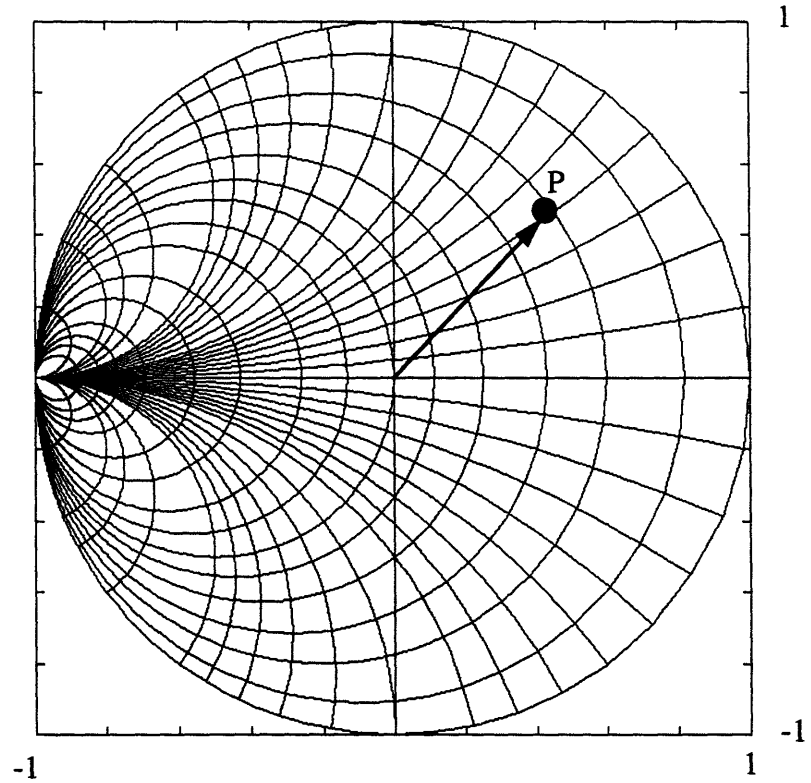

Fig.8: Admittance Smith Chart

The length of the arrow in Fig.7 represents the magnitude of the voltage or current reflection according to EQ34 i.e V_{ts}/V_{tl}. It follows that the magnitude of the reflection factor (i.e the length of the arrow) can similarly be expressed as a function of the transmitted and reflected power:

EQ47

$$|\Gamma| = \sqrt{\frac{P_{out}}{P_{in}}} \quad .$$

This relation is very useful since (as we will see in chapter 4) the reflected power is easily measurable with a special device called a reflection bridge. Therefore, by measuring the complex power reflection coefficient of an element or device yields the impedance value.

In NMR, the Smith chart is a useful tool to tune and match coils to the characteristic transmission line impedance Z_0. (i.e. Γ should be zero at the frequency of interest)

Since the coil impedance itself has a relatively small real part and a relatively large imaginary part, a transformation network is needed. The following chapter will introduce the basics of this transformation.

2.3 Matching of MR coils

Most of the common MRI coils are single wire loops or surface coils which will be used here to describe the concept of matching. The approx. $\pi/2$ phase shift between the sinusoidal current and voltage (as a direct consequence of the voltage induction law) in a coil is expressed by the complex impedance,

EQ48

$$Z_{coil} = r + j\omega L \quad ,$$

where L is a proportional constant between magnetic flux and the current through the coil (i.e. the inductance), ω the angular frequency of the sinusoidal voltage and current applied and r the resistive part that models losses of the sample and the coil itself. It is clear that if we connect the coil to a transmission line with a characteristic impedance Z_0, there will be a reflection and the energy transfer from the RF amplifier/receiver to/from the coil will be inefficient. What is needed is an interface between the coil and the transmitter/receiver to transforms Z_{coil} into Z_0. The Smith chart can be used to derive and understand these interfaces.

The transformation of Z_{coil} yields the reflection represented by point P_1 in Fig.9. A variable capacitor C_t connected in parallel with the coil yields the

impedance,

EQ49

$$Z_p = \frac{r + j\omega L}{1 - \omega^2 L C_t + jr\omega C_t} \quad .$$

By varying C_t both the real and imaginary part of Z_p can be varied. The locus A in Fig.9 shows this. Two particular values of C_t yield a real part of Z_p that is equal to Z_0 (P_2 and P_3 in Fig.9).

EQ50

$$Z_p(C_{t1}) = Z_0 + jX \qquad \text{and} \qquad Z_p(C_{t2}) = Z_0 - jX \quad .$$

Adding an element (i.e. a capacitor for the C_{t1} case and an inductor for the C_{t2} case) which cancels jX yields an overall impedance of Z_0 and thus a reflection coefficient of 0 (locus B_1 and B_2 in Fig.z). The locus B_1 represents the cancellation of jX with a series capacitor and thus the curve starts at the +1 point in the complex reflection plane (i.e. C_m=0). For the cancelation of $-jX$ with an inductor, the curve starts at P_3 since an serial inductance of 0 does not change Z_p.

Note that above equations are not normalized.

This is the matched condition where all the power from the source is dissipated in r (assuming ideal inductors and capacitors). Fig.9 shows the development of the matching condition in the reflection plane.

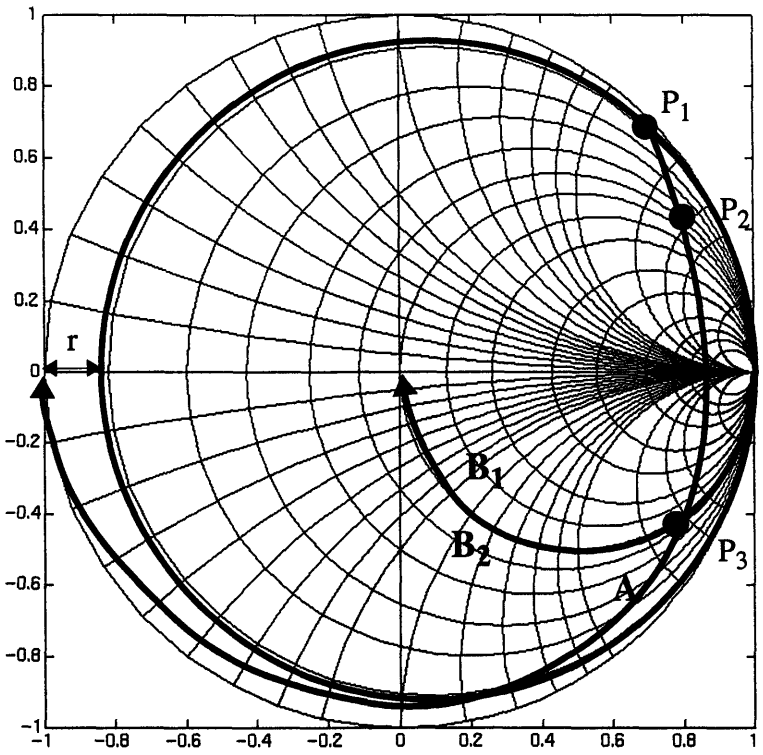

Fig.9: Matching corresponding to the circuits Fig.10a and Fig.10b

Notice that the graphs represent increasing element values in the direction of the arrow. For example curve A represents the parallel capacitor C_t. Clearly if C_t increases towards infinity the impedance Z_p decreases towards 0 and thus $\Gamma \rightarrow -1$ which is the position where the arrow points. The design with the Smith chart provides more insight than tedious complex algebra.

There are four possible networks for transforming the coil impedance to a characteristic transmission line impedance. Each of these circuits can be developed in a similar way as described above. Fig.10 shows the four basic

circuits:

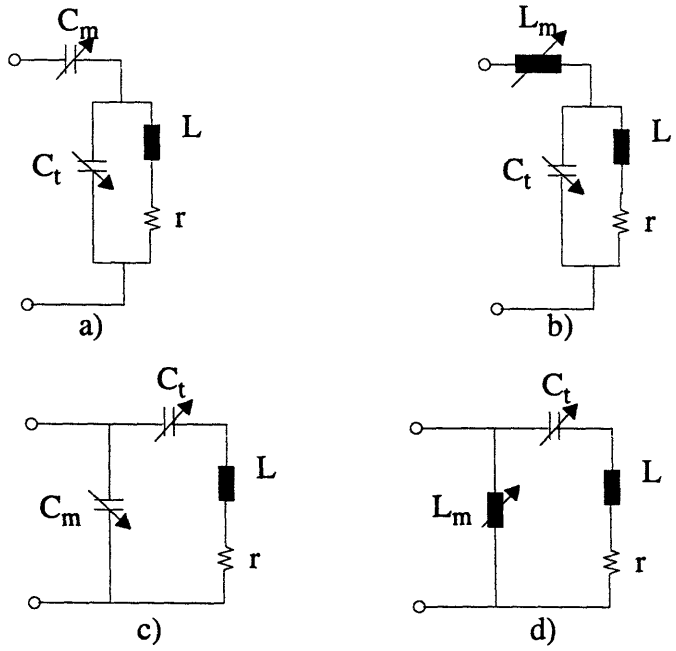

Fig.10: Four basic matching schemes

The knowledge of the basic concept of matching a basic resonant circuit will be useful later when we discuss the Birdcage resonator. There it can be seen that resonant modes can be understood as a superposition of parallel (upper two circuits in Fig.10) or serial LC circuits (lower two circuits in Fig.10). Then it will be clear that the matching scheme as we derived it before selects the serial or parallel mode.

3. The Birdcage resonator

3.1 Motivation

Using a simple Surface coil for imaging has a the disadvantage that the RF field strength has a strong spatial dependency and thus different signal intensities on the MR image for different local points in space. To see this we can use Biot-Savarts law of magnetostatics. Assume a wire loop with a constant current I_0 (this current is in the form of $A\cos(\omega_0 t - \varphi)$). Since the wave length is much larger than the actual size of the wire loop we will assume static conditions. The surface coil configuration is depicted in the following figure:

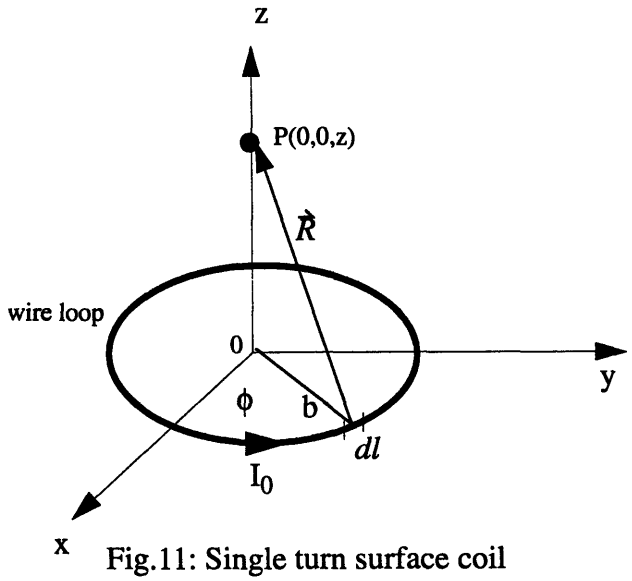

Fig.11: Single turn surface coil

The object that is to be imaged is placed in the region z>0 where P is an arbitrary point chosen for simplicity along the z axis. We can apply the Biot-Savart law for the above configuration,

EQ51

$$\vec{B} = \frac{\mu_0 I_0}{4\pi} \oint_C \frac{dl \times a_R}{R^2} \quad ,$$

where μ_0 is the permeability of free space, a_R the unit vector for the radius in

cylindrical coordinates, I_0 the current through the wire loop, R the distance between the differential length *dl* and the point of interest P. The contour integral has to be evaluated along the wire loop. Rewriting EQ51 yields,

EQ52

$$\vec{B} = \oint_C d\vec{B} \quad ,$$

with

EQ53

$$d\vec{B} = \frac{\mu_0 I_0}{4\pi}\left(\frac{d\vec{l} \times \vec{R}}{R^3}\right) \quad .$$

Using cylindrical coordinates, *dl* and $\vec{R}$ can be expressed as

EQ54

$$d\vec{l} = a_\phi b d\phi \quad ,$$

$$\vec{R} = a_z z - a_r b \quad ,$$

where a_r, a_ϕ, a_z are the unit vectors in cylindrical coordinates. Note that the vector $\vec{R}$ is pointing towards the origin of the coordinate system and thus the negative sign in EQ54b. To calculate the differential magnetic flux density, $d\vec{B}$, we calculate the cross product:

EQ55

$$d\vec{l} \times \vec{R} = a_\phi b d\phi \times (a_z z - a_r b) = \begin{vmatrix} a_r & a_\phi & a_z \\ 0 & b d\phi & 0 z \\ -b & 0 & z \end{vmatrix} = a_r b z d\phi + a_z b^2 d\phi \quad .$$

Substituting EQ55 into EQ53 and EQ52 yields,

EQ56

$$\vec{B} = \frac{\mu_0 I_0}{4\pi}\oint_C \frac{a_r bz d\phi + a_z b^2 d\phi}{(b^2+z^2)^{3/2}} = \frac{\mu_0 I_0}{4\pi}\left(\oint_0^{2\pi} \frac{a_r bz d\phi}{(b^2+z^2)^{3/2}} + \oint_0^{2\pi} \frac{a_z b^2 d\phi}{(b^2+z^2)^{3/2}}\right)$$

$$\Big\| \quad 0$$

The first part in EQ56 is zero since the a_r component is canceled by the contribution on the opposite side of *dl.* EQ56 evaluated around the wire loop (i.e. form 0 to 2π) yields

EQ57

$$\vec{B} = a_z \frac{\mu_0 I_0 b^2}{2(z^2+b^2)^{3/2}} .$$

Fig.12 shows the flux density for a surface coil with a radius of 5cm and a current of 2 A.

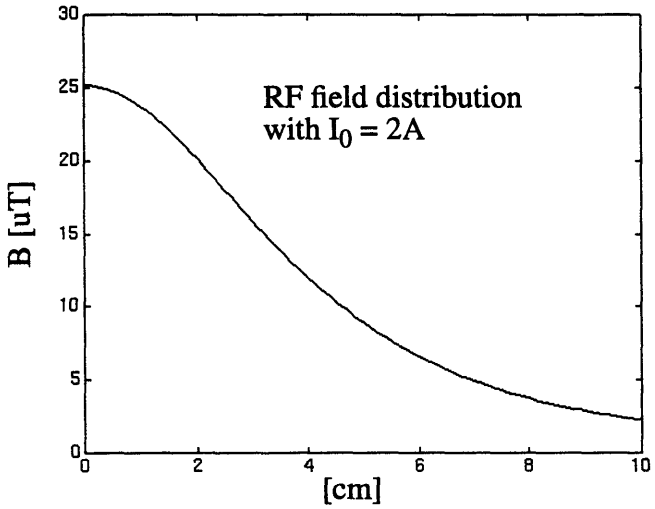

Fig.12: Flux density of the single turn surface coil with 5cm radius

The B field intensity is directly related to the nutation frequency (see chap. 1) of the spins and thus to the $\pi/2$ pulse. We can clearly see the spatial depen-

dency of the field intensity along the z-axis and thus the distance from the surface of the object to the points of interest inside the object. Images taken with such a surface coil will show different intensities for points with equal spin density. Therefore surface coil images are much harder to analyze and are only useful for limited fields of view.

3.2 Principle of the Birdcage Resonator

An obvious approach to improving the spatial characteristic of the surface coil configuration from the previous section, is to use a second wire loop a distance apart from the first one, with the current in the same direction. The B field between the wire loops shows less fluctuation than with the single loop coil. This configuration is depicted in the next figure:

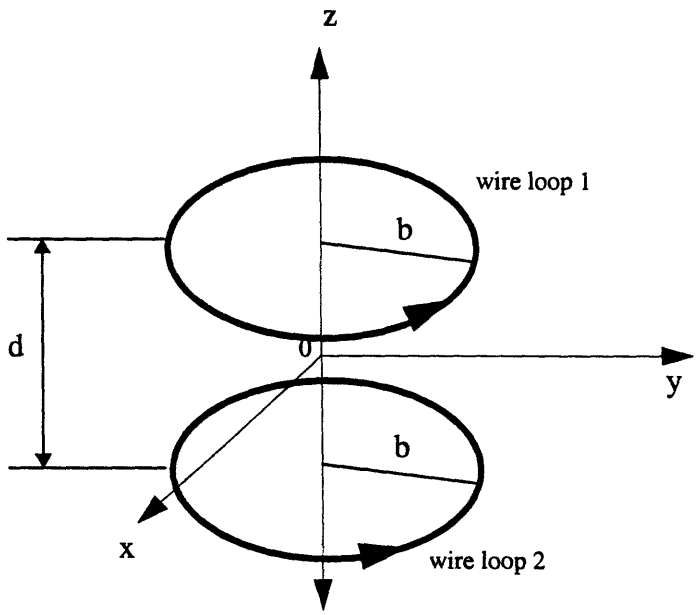

Fig.13: Two current rings form a Helmholz coil

We can use EQ57 and the principle of superposition to get an idea about the field inside these two wire loops. Fig.14 shows the field intensity for two wire loops separated by 6cm. Note that this is the plot of the intensities along the z

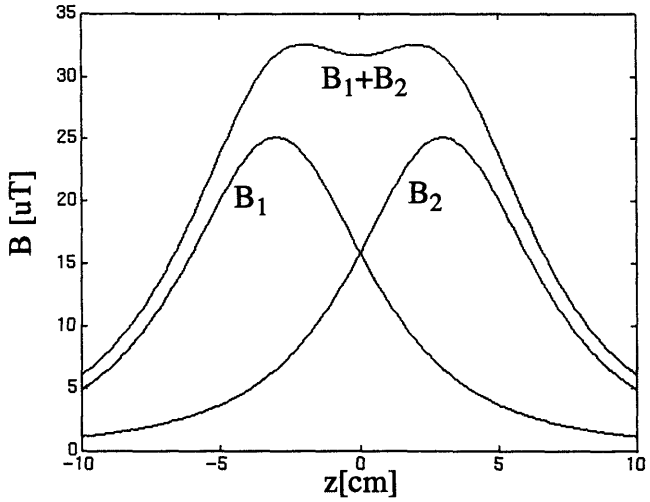

Fig.14: Flux density profile for the Helmholz coil

axis. (i.e. x=y=0) For intensities with $x, y \neq 0$ the field has even larger humps than depicted in Fig.14. Stretching the coil along the y axis would certainly improve the situation for $y \neq 0$. That would result in a setup depicted in Fig.15:

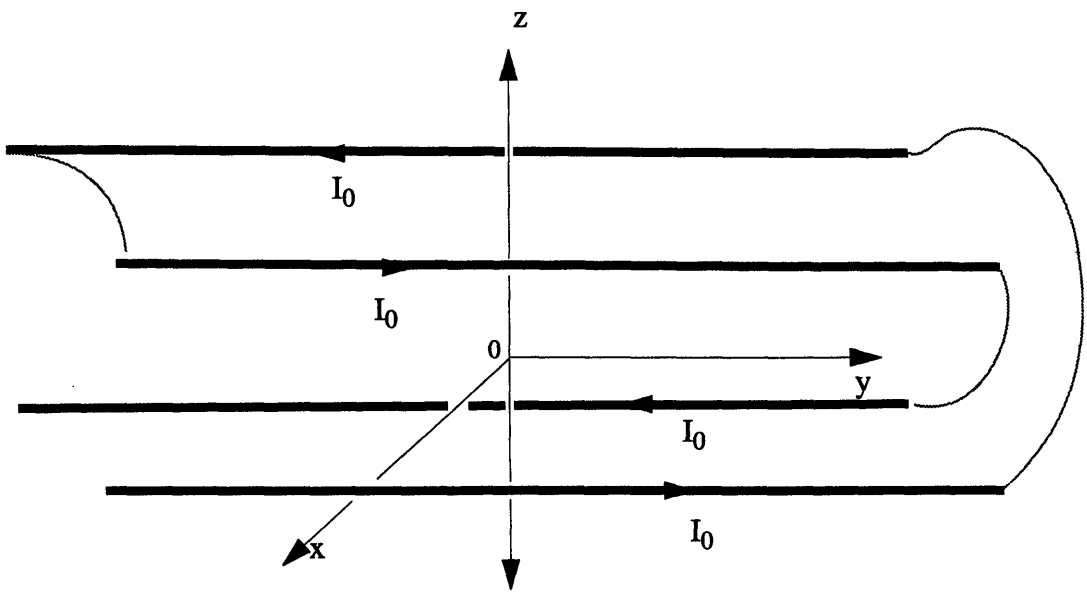

Fig.15: Stretched ring pair yields saddle coil

Since all the current intensities I_0 are the same we could connect the wires above in the right way to get a setup which is known as the saddle coil. This design must have a better field distribution than the two wire loop setup, but that the humps along the x and z axis are still apparent. A setup with more than 4 wires and different currents I_0, would improve the B field characteristic further.

The saddle coil, as we will see later, can be viewed as a 6 mesh Birdcage resonator. A Birdcage resonator is simply a ladder network which is wrapped around a non metallic cylinder[2]. Fig.16 illustrates this:

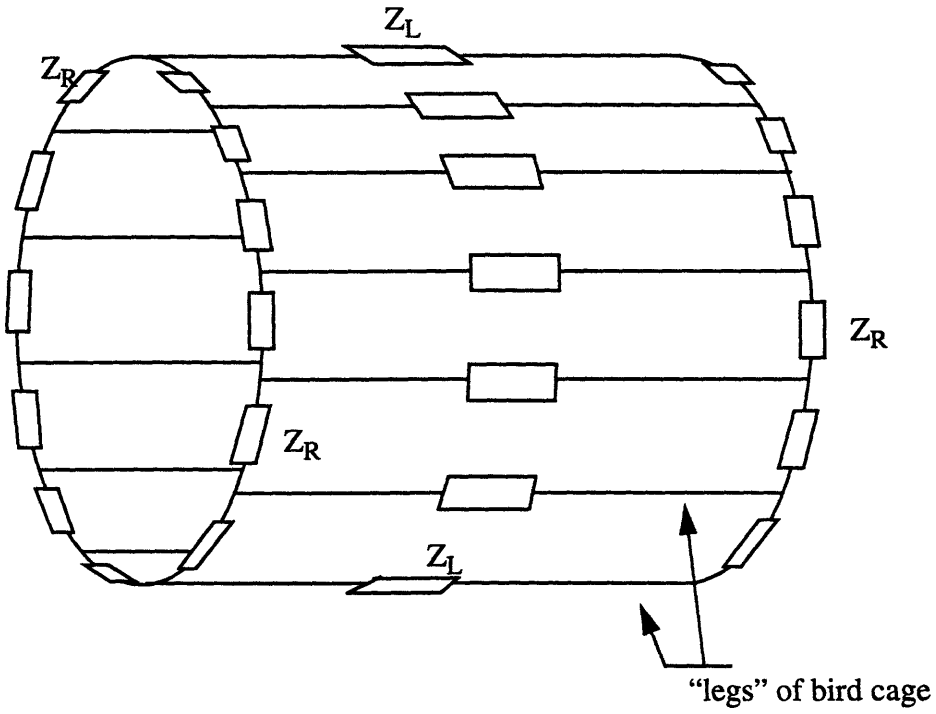

Fig.16: A cylindrical ladder network is a Birdcage resonator

The object to be measured is located inside the resonator. The complex impedances Z_L and Z_R represent either lumped elements or distributed impedances or both. In most cases the "legs" of the Birdcage are simple wires or thin shims. Then a part of Z_L would count for the inductance of this wire or shim.

It is important to note that Z_R and Z_L are not necessarily lumped elements, they represent the physical construction of the Birdcage. The currents through each of the legs contribute to the overall magnetic field distribution according to the superposition principle.

3.3 Resonance frequencies of the Birdcage resonator

Our objective in this section is to find an expression for the resonant frequencies of the Birdcage from which we can then find the leg currents that create the magnetic field inside the resonator. Two approaches will be used. First we derive the currents from Kirchhoff's laws with the appropriate boundary conditions and then we will compare it to a transmission line approach [2]. Of course the two methods should deliver the same results.

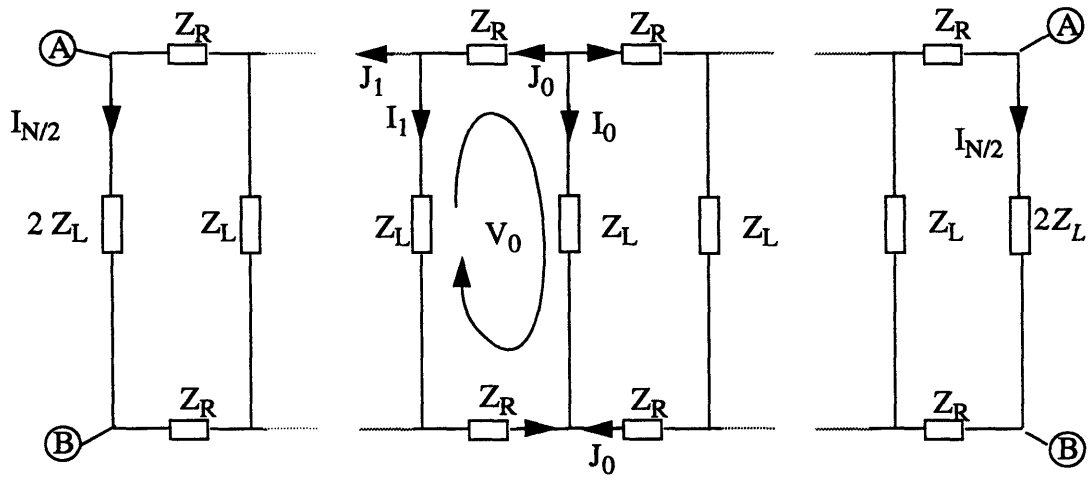

Fig.17: Equivalent circuit for a Birdcage resonator

The network in Fig.17 represents the resonator which has been cut "in the middle" of impedance Z_L at leg position N/2. N is the total number of legs. Note that the connection of the points labeled A and B yields the original resonator. Thus the impedances at point N/2 are twice as high as Z_L. We recognize that the ladder network is symmetric and thus currents and voltages on the right side of leg 0 are the same as currents and voltages on the left side of leg 0. Therefore the indices used to determine voltages and currents can be applied on either side. Considering an initial current I_0 in the leg at position n=0, and using Kirchoffs relation:

EQ58

$$\sum_k V_k = 0 \quad , \quad \sum_k I_k = 0 \ .$$

We can see that $J_0 = -I_0/2$. Assuming the knowledge of $Z_L$and Z_R and using Kirchhoffs voltages law we can write:

EQ59

$$I_0 Z_L - 2J_0 Z_R - I_1 Z_L = 0 \ ,$$

and

EQ60

$$J_1 = J_0 - I_1 \quad .$$

Combining EQ59 and EQ 60 yields:

EQ61

$$I_1 = I_0\left(1 + \frac{Z_R}{Z_L}\right) \ ,$$

and

EQ62

$$J_1 = -I_0\left(\frac{3}{2} + \frac{Z_R}{Z_L}\right) \ .$$

EQ61 and EQ62 can be solved recursively for any index n. The recursion for-

mulae can be obtained by applying Kirchhoffs law to the next meshes using the knowledge of the previous currents. This yields the following recursive equations:

EQ63

$$I_{n+1} = I_n - 2J_n \frac{Z_R}{Z_L} \quad ,$$

$$J_{n+1} = J_n - I_{n+1} \quad .$$

Substituting $k = Z_R/Z_L$ and carrying out the above recursion, the currents I_n and J_n can be expressed as a polynomial in k

EQ64

$$J_n(k) = -\frac{I_0}{2} \sum_{i=0}^{n} d_{n,i} \cdot k^i \quad ,$$

$$I_n(k) = I_0 \sum_{i=0}^{n} c_{n,i} \cdot k^i \quad .$$

Appendix A shows how to calculate the coefficients c_i and d_i. At this point, it is only important to note that the current in each leg can be represented by a polynomial function and the coefficients can be computed. The argument of the polynomials (i.e. k) is directly related to the impedances Z_R and Z_L (i.e. Z_R/Z_L). Thus the polynomials are totally independent of the physical construction of the Birdcage. The only constraint is that Z_R and Z_L are equal in every section of the resonator. Notice that the Birdcage is still "open" i.e. the ends of the ladder network of Fig.17 have not been connected yet and N (the number of legs) is still undetermined. Before reconnecting the resonator, we have to account for the doubled impedances at the end of the ladder, for the calculation of the polynomial functions $I_{N/2}(k)$ and $J_{N/2}(k)$. Appendix A_1 shows this explicitly for a 12 leg Birdcage resonator.

Define positive indices for currents and voltages on the right side of the ladder network in Fig.17 and negative indices for voltages and currents on the left side. By Defining V_n as the potential voltage between two impedances Z_L and due to symmetry it follows that:

EQ65

$$V_n = V_{-n} \quad ,$$

and consequently this has to be true for n=N/2 and n=-N/2. Now consider to connect the points A and B (i.e. closing the ladder network to get the original Birdcage). Fig. 18 depicts this "closing procedure"

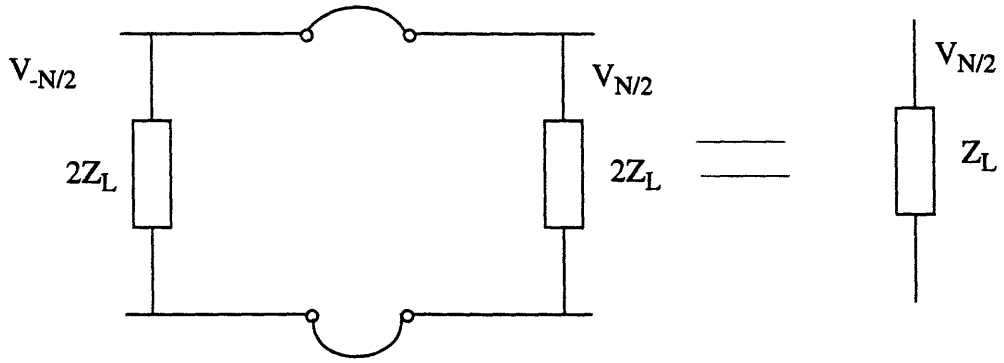

Fig.18: Reconnecting the ladder network to yield original Birdcage

From EQ65 we know that the two potentials $V_{-N/2}$ and $V_{N/2}$ are equal. Thus we can say that the currents $J_{N/2}$ and $J_{-N/2}$ have to be zero. This applies a boundary condition to the polynomials which represent $J_{N/2}$ and $J_{-N/2}$ i.e.:

EQ66

$$J_{N/2}(k) = J_{-N/2}(k) = 0 \quad .$$

Since this polynomial has the order N/2, a maximum of N/2 roots are possible i.e. only N/2 k values satisfy EQ66. No information has been given about Z_R and Z_L, thus EQ66 is valid for any N mesh Birdcage resonator.

Considering a low pass Birdcage (i.e. a resonator with inductive ring elements and capacitive leg elements) with known parameters Z_R and Z_L and assuming the most simple model (i.e. the ring impedance is a pure inductor $Z_R = j\omega L$ and the leg impedance is a pure capacitor $Z_L = -j/(\omega C)$ we can express k as:

EQ67

$$k = \frac{Z_R}{Z_L} = -\omega^2 LC \quad .$$

Since k is restricted to N/2 distinct (k_1,k_2,k_3,..$k_{N/2}$) values and L and C are constant (i.e. the physical inductors and capacitors of the resonator), the boundary conditions of EQ66 can only be met if the frequency ω is:

EQ68

$$\omega_j = \sqrt{-\frac{k_j}{LC}} \quad ,$$

where k_j are the roots of $J_{N/2}(k)$. The roots are certainly the same on the right and left side of the ladder network and can be viewed as a two fold degeneracy [3]. In section 3.3 we will use numerical methods to verify the resonance frequencies of this particular Birdcage..

This simple resonator has been described earlier [2] with a transmission line model. The results of the two approaches are compared.

The resonance frequencies in [2] are:

EQ69

$$\omega = \frac{2}{\sqrt{L_1 C}} \sin\frac{\pi M}{N} \quad ,$$

where M corresponds to the mode (i.e. j in our notation), L_1 is twice the ring inductance of one segment of a low pass Birdcage (i.e. L in our notation), N the number of legs and C the value of the leg capacitor.

EQ68 and EQ69 should yield the same resonance frequencies since the same elements are assumed. (i.e. ring impedances are inductors with value L = 1/ $2L_1$ and leg impedances are capacitors with value C)

Changing EQ69 to our notation (i.e. $L_1 = 2L$) yields:

EQ70

$$\omega_j = \sqrt{\frac{2}{LC}} \sin\frac{\pi j}{N} \quad .$$

Note that j refers to the mode as in EQ68.

Comparing EQ68 and EQ70 yields:

EQ71

$$\sqrt{2}\sin\frac{\pi j}{N} = \sqrt{-k_j} \quad .$$

A verification of EQ71 can be done by using the values for k_j from Appendix A_1 for the 12 mesh Birdcage (i.e. N=12). The following table shows the results:

Table 1:
Verification of polynomial approach
by comparison with transmission line
approach of Hayes et al [1]

mode j	$\sqrt{2}\sin\frac{\pi j}{N}$	$\sqrt{-k_j}$
1	0.3660	0.3660
2	0.7071	0.7071
3	1.0000	1.0000
4	1.2247	1.2247
5	1.3360	1.3360
6	1.4142	1.4142

The polynomial approach seems to be a little more complicated than the simple sine function from Hayes et al [2]. The concept however can be used for any kind of leg and ring impedances and is therefore more general.

In order to get a reasonable RF field homogeneity it is advisable to design Birdcages with more legs. As a consequence, adjacent meshes are spatially close and therefore coupling between the leg wires may exist. An inductance that models the self and mutual inductances of the legs can be added to get a more exact model of the Birdcage. This is suggested in [2] but there is no follow up. In [3] the model for the mutual inductance has been included and the resonance frequencies are obtained by solving an eigenvalue problem. Here again the polynomial approach should yield the same result.

The new Birdcage model changes the leg impedance Z_L to a series LC circuit:

EQ72

$$Z_L = j\left(\omega L_1 - \frac{1}{\omega C}\right) \ ,$$

where L_1 is the inductor which models the self and mutual inductance of the legs. The ratio $Z_R/Z_L = k$ changes to:

EQ73

$$k = \frac{\omega^2 LC}{\omega^2 L_1 C - 1} \ .$$

Remembering that the boundary condition for $J_{N/2}(k)$ yields N/2 solutions for k and thus N/2 resonance frequencies. EQ73 can be solved for ω,

EQ74

$$\omega_j = \sqrt{\frac{k_j}{C\,(L - k_j L_1)}} \ .$$

Since k_j is the same for any N mesh resonator, introducing L_1results in a shift of resonances to higher frequencies, which is consistent with [3].

3.3.1 Birdcage design procedure including mutual inductance

From a practical perspective, it is rather difficult to exactly measure the inductances of L and L_1. This knowledge, however, is needed to predict the resonance frequencies with EQ74. Since it is much easier to measure the resonance frequencies of a Birdcage, the resonance spectra can be used to determine L and L_1. Solving EQ74 for L and L_1 yields,

EQ75

$$L = \frac{k_1}{\omega_1^2 C}\left(\frac{k_2\omega_1^2 - k_1\omega_2^2}{\omega_2^2(k_2 - k_1)} - 1\right) ,$$

EQ76

$$L_1 = \frac{k_2\omega_1^2 - k_1\omega_2^2}{C(k_2 - k_1)(\omega_1\omega_2)^2} ,$$

where k_1 and k_2 are any two roots of the polynomial $J_{N/2}(k)$, ω_1 and ω_2 the corresponding measured resonance frequencies.

Since the capacitor values C are easy to measure, the following low pass Birdcage design procedure is applicable:

1. Construct an N mesh low pass Birdcage with arbitrary capacitor value C_{start}.
2. Measure the N/2 resonance frequencies
4. Use EQ77 (derived from EQ24,EQ25,EQ26) to determine C_d for the desired frequencyω_d and desired mode m:

EQ77

$$C_d = C_{\text{start}} \frac{-k_m \omega_1^2}{\omega_d^2 [k_1 (a-1) - k_m a]} \quad ,$$

with the variable a defined as:

EQ78

$$a = \frac{k_2 \omega_1^2 - k_1 \omega_2^2}{\omega_2^2 (k_2 - k_1)} \quad .$$

3.3.2 Comparison of polynomial approach with [3]

As a verification of the polynomial approach (including the leg inductors) we use the resonance frequencies obtained by [3].

His resonator is a 8 mesh low pass Birdcage and his equation [6] for the resonant frequencies is:

EQ79

$$\omega_j^2 = 2\omega_a^2 [1 - \cos(2\pi j/N)] / [1 - 2(\omega_a/\omega_b)^2 \cos 2\pi (j/N)] \quad ,$$

where $\sqrt{2}\omega_a$ is the resonance frequency of a single mesh and ω_b is the resonant frequency of a single leg. ω_a and ω_b have to be adjusted to yield the 4 resonant frequencies observed by the experiment ([3] page 53)

for j=2 EQ79 reduces to

EQ80

$$\omega_2^2 = 2\omega_a^2 \quad .$$

Substituting ω_a and ω_1 into EQ79 yields ω_b

EQ81

$$\omega_b^2 = \frac{\omega_1^2\omega_2^2\cos(\pi/4)}{\omega_1^2 - \omega_2^2(1-\cos(\pi/4))} \quad .$$

Using the calculated frequencies ω_1 and ω_2 ([3] page 53), EQ80 and EQ81 (which are derived from his equation [6])the following resonant frequencies are calculated:

Table 2:
resonant frequencies calculated with Tropp's equation [6]

j	f_j [MHz]
1	34.7
2	54.5
3	63.0
4	65.3

With the parameters ω_a and ω_b we can extract the inductance of the ring inductor and the mutual inductance between the legs ([3] page 52)

EQ82

$$M = 1/\omega_b^2 \ ,$$

and

EQ83

$$L = 1/(2\omega_a C) - M \ ,$$

where M is the mutual inductance between the legs, L the inductance of the ring inductor and C is the given leg capacitor with value 62pF. Note that in the polynomial approach we used the variable L_1 to express the mutual inductance between the legs.

At this point we have determined the resonant frequencies ω_3 and ω_4, the ring inductances and the mutual inductances for a 8 mesh low pass Birdcage with the method proposed in [3].

Now the polynomial approach is used to determine the resonance frequencies of the same 8 mesh low pass resonator. It is sufficient to show that with the same physical parameters (i.e. leg capacitor C, ring inductor L and mutual inductance M) the polynomial method yields the same resonance frequencies. First we need to find the polynomial $J_4(k)$ of the 4 mesh ladder network with the same procedure as we did it for the 12 mesh Birdcage example in Appendix A_1. Executing the procedure and applying the boundary condition yields:

EQ84

$$J_4(k) = 8k^4 + 40k^3 + 68k^2 + 44k + 8 = 0 \ .$$

The solutions of EQ84 are:

Table 3:
roots of $J_4(k)$ for 8 mesh Birdcage

j	k_j
1	-0.2929
2	-1.0000
3	-1.7071
4	-2.0000

Again, these roots are the same for all 8 mesh Birdcages no matter what impedances we use. The system is constrained to a low pass Birdcage by defining $Z_R = j\omega L$ and $Z_L = j\omega M + 1/(j\omega C)$. Using the parameters calculated from [3] (i.e. L, C, M) and applying EQ74 yields the resonant frequencies using our method.

Note that we substitute L_1 in EQ74 with M to account for the different nota-

tion. Table 4 shows the results:

Table 4:
resonant frequencies using polynomial approach

j	f_j [MHz]
1	34.7
2	54.5
3	63.0
4	65.3

By comparing table 2 and table 4 we can see that the two methods yield exactly the same results.

3.3.3 Additional initial conditions

The derivation of the N/2 resonance frequencies in the previous section is based on the assumption that the current I_0 is present at leg 0. With this initial condition, we derived the resonance frequencies for a general Birdcage. Let us use the same concept to derive the resonance frequency of a simple parallel circuit of two pure imaginary impedances Z_1 and Z_2 as shown in Fig.19.

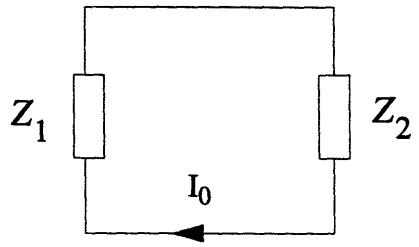

Fig.19:
parallel circuit to show concept of high impedance mode

As we did for the Birdcage we assume a given current I_0 and apply Kirchhoffs law again:

EQ85

$$I_0(Z_1 + Z_2) = 0 \ .$$

Using the substitution $Z_1/Z_2 = k$ we get:

EQ86

$$I_0(k+1) = 0 \ ,$$

which can be viewed as a polynomial in k of degree 1. The solution of course is $k_1 = -1$. If Z_1 is a capacitor C and Z_2 an inductor L we get:

EQ87

$$\frac{Z_1}{Z_2} = -\frac{1}{\omega^2 LC} = -1 \ ,$$

which yields of course the resonance frequency of a parallel LC circuit. Since the system is resonating unperturbed (i.e. no energy is dissipated) it can be viewed as a high impedance (infinite resistance) circuit. This parallel LC circuit example should make clear, that the assumption of the initial current I_0 yields the high impedance resonance frequency. Therefore the derivation of the Birdcage resonant frequencies in the previous chapter yields high impedance modes.

If we now reconsider the transmission line model, we know that it acts as a low impedance at certain frequencies. (i.e. reflection factors of -1) This is easily shown by considering EQ34 in chapter 2.2.6:

EQ88

$$\Gamma(z) = \frac{V_{ts}}{V_{tl}} e^{2\gamma z} \ .$$

Consider the position z to be fixed and the complex propagation constant

$\gamma = j\beta = j\omega/v$ the reflection as a function of frequency is,

EQ89

$$\Gamma(\omega) = \frac{V_{ts}}{V_{tl}} e^{2j\omega z/v} \quad ,$$

where v is the phase velocity.

Clearly EQ89 crosses low and high impedance points (i.e. -1 and 1) in the complex reflection plane as a function of the frequency ω . Since the ladder network which models the Birdcage is similar to the transmission line model of Fig.2, we can intuitively conclude that the Birdcage must have resonant frequencies which correspond to low impedances or, with the LC analogy, series resonant modes.

Let us again consider the ladder network in Fig.17. If the input impedance across the leg impedance at position 0 has to be zero (corresponding to a reflection factor of -1), then there is no current present in leg 0. Therefore the initial condition is,

EQ90

$$I_0 = 0 \quad ,$$

and with connecting a current source across leg 0

EQ91

$$J_0 = \frac{1}{2} \quad .$$

Note that J_0 can be any constant since the roots of the polynomials are not affected by a constant multiplier. Here we use 1/2 for convenience. With these initial conditions we use EQ63 again to recursively compute the coefficients for the J and I polynomials. The resulting coefficients are shown in Appendix A_2.

Applying the same modification procedure for the $I_{N/2}$ leg, as done for the

'high impedance' case, yields the ring current $J_{N/2}$. Applying the same boundary condition as before (i.e. $J_{N/2}=0$) for a 12 mesh Birdcage we get:

EQ92

$$J_6(k) = \frac{1}{2}(32k^6 + 192k^5 + 432k^4 + 448k^3 + 210k^2 + 36k + 1) = 0 \ .$$

The k values which satisfy EQ92, shown in Appendix A_1, are related to the frequencies with zero input impedance (and hence the name low impedance resonance frequencies).

The conclusion therefore is that an N-mesh Birdcage resonator has a total of N resonance frequencies, i.e. N/2 high impedance and N/2 low impedance resonances. The selection of either mode can be done with the matching circuit. (as in the case for parallel and serial LC circuit; see chapter 2.3)

3.4 Current distribution

The RF-field distribution inside the bird cage resonator is a superposition of the induced magnetic field due to the current flux through each individual leg. (see 3.1) In order to compute the magnitude and phase of this field, the currents must be known. We have already derived an expression for these currents I_n in order to arrive at the resonance frequencies (i.e. the polynomial functions in Z_R/Z_L).

Each polynomial I_n represents the current flux through the leg at the angular position $2\pi n/N$, where n is the leg number and N the total number of legs as shown in Fig.20.

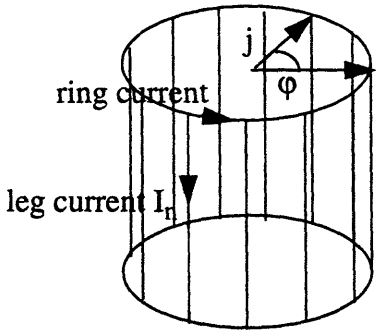

Fig.20:
Definition of angular position φ

Suppose we express the current as:

EQ93

$$I_n = I_0 u(n\varphi) \quad ,$$

where $u(x)$ is an unknown function of the current distribution and φ is $2\pi/N$ (with N the total number of legs).

From EQ61, the current through the first leg (I_1) is

EQ94

$$I_1 = I_0 (1 + k) .$$

Applying EQ93 to the first leg and combining combine EQ93 and EQ94,

EQ95

$$I_0 (1 + k) = I_0 (u\varphi) \quad .$$

Solving EQ95 for k yields,

EQ96

$$k_i = u_i (\varphi) - 1 \quad .$$

Note the index i is introduced since we know that only N/2 k values and thus N/2 distinct unknown functions are possible. Replacing k_i in EQ64b (i.e. the polynomials for the leg currents) with EQ96 yields to the following set of polynomials:

EQ97

$$u_i(0) = 1$$

$$u_i(\varphi) = 1 + (u_i(\varphi) - 1)$$

$$u_i(2\varphi) = 1 + 4(u_i(\varphi) - 1) + 2(u_i(\varphi) - 1)^2$$

$$u_i(3\varphi) = 1 + 9(u_i(\varphi) - 1) + 12(u_i(\varphi) - 1)^2 + 4(u_i(\varphi) - 1)^3$$

.

.

.

Expanding and rewriting yields:

EQ98

$$u_i(0) = 1$$

$$u_i(\varphi) = u_i(\varphi)$$

$$u_i(2\varphi) = -1 + 2u_i^2(\varphi)$$

$$u_i(3\varphi) = -3u_i(\varphi) + 4u_i^3(\varphi)$$

$$u_i(4\varphi) = 1 - 8u_i^2(\varphi) + 8u_i^4(\varphi)$$

or

EQ99

$$u_i(n\varphi) = \sum_l^n a_l [u(\varphi)]^l$$

By inspection, we see that the coefficients in EQ99 represent a set of Cheby-

chev polynomials[9]. They are defined as:

EQ100

$$T_n(x) = \cos(n\varphi) \qquad \text{with} \quad x = \cos(\varphi) \ .$$

The Chebychev polynomials can be derived from the identity[9]:

EQ101

$$\cos((n+1)\varphi) + \cos((n-1)\varphi) = 2\cos(\varphi)\cos(n\varphi) \ .$$

The coefficients in EQ100 are equivalent with the coefficients obtained in EQ98. Thus unknown functions $u_i(\varphi)$ must becos $(i\varphi)$.

for i=1..N/2.

By summarizing above steps the leg current distribution for a Birdcage tuned to the high impedance modes is,

EQ102

$$I_n = I_0 \cos(n\varphi) \qquad \text{with} \quad \varphi = \frac{2\pi m}{N} \ ,$$

where N is the total number of legs and m = 1..N/2.

The concept of splitting the leg impedance at leg position N/2 and using the boundary condition $J_{N/2}(k)=0$, implies that the leg current distribution must be an even function around N/2.

What is the current distribution when the Birdcage is tune to the low impedance mode?

In this mode the current through the first leg is zero and that the current distribution function has to be even around both the first leg and the leg at N/2. (symmetry argument) Let us now consider a given current $I_{N/2}$ at leg position

N/2. If we split the resonator at this position, we are left with half of $I_{N/2}$ and a doubled leg impedance. Fig.21 illustrates this:

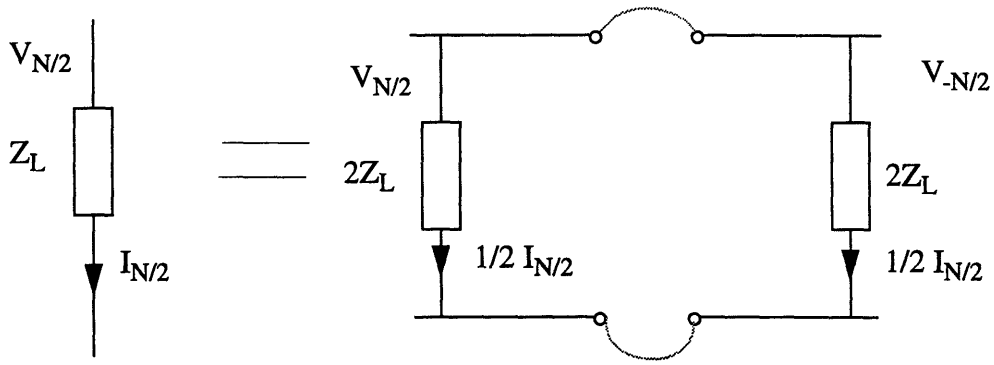

Fig.21: Splitting of leg at N/2 to show current distribution in low impedance mode

With the N/2 mesh shown in Fig.22:

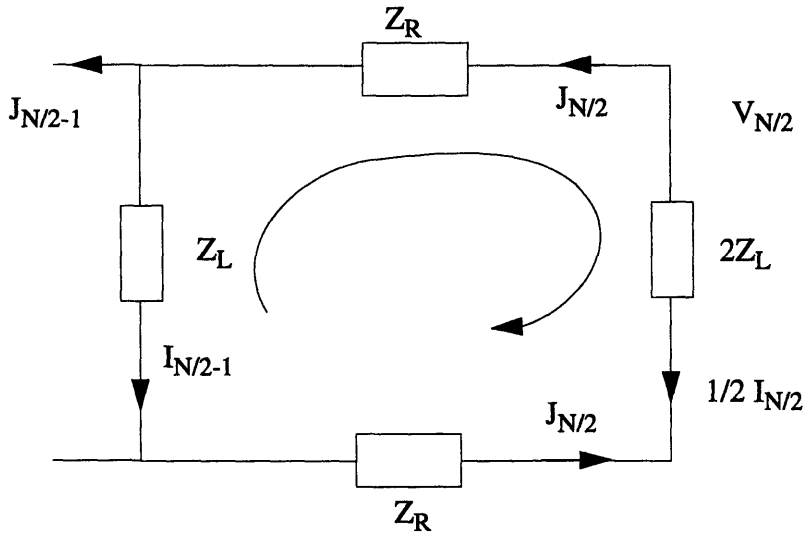

Fig.22: Mesh at leg N/2

Writing down Kirchhoffs law:

EQ103

$$I_{N/2}Z_L - 2Z_R J_{N/2} - I_{N/2-1}Z_L = 0 \quad .$$

and $J_{N/2} = -\frac{1}{2} I_{N/2}$ we get:

EQ104

$$I_{N/2-1} = I_{N/2}(1+k) \quad ,$$

and

EQ105

$$J_{N/2-1} = I_{N/2}\left(\frac{3}{2}+k\right) \quad .$$

EQ104 and EQ105 are equivalent with EQ61 and EQ62 except for 'backwards running' indices. Therefore the same recursion can be applied and the same polynomials as in EQ64 result (except the n index). Thus we can write,

EQ106

$$I_n(k) = \frac{I_{N/2}}{2} \sum_{i=0}^{N/2-n} c_{N/2-n,i} \cdot k^i$$

$$J_n(k) = \frac{I_{N/2}}{2} \sum_{i=0}^{N/2-n} d_{N/2-n,i} \cdot k^i$$

where the coefficients $c_{n,i}$ and $d_{n,i}$ are shown in Appendix A_1.

We can now use the zero current in the first leg as the boundary condition. Doing this yields a set of k values which satisfy this boundary condition. For a 12 mesh Birdcage these k values are identical with the ones calculated in Appendix A_2.

In the previous section we have shown that the evaluation of the polynomial at leg position n yields a cosine function.

For the low impedance modes we have shown that the same polynomials can be used if the starting point of the recursion is N/2. Thus the current distribution has to have a cosine shape starting at N/2. Since the zero current constraint has to be met for the first leg the current distribution function has to be

$I_{N/2}\cos\left([N/2-i]\,\varphi/2\right)$ with i being the leg number and $\varphi = 2\pi/N$

This expression can be written as,

EQ107

$$I_i = -I_{N/2}\sin\left(\frac{\varphi}{2}i\right) \quad .$$

Since we have again N/2 polynomial roots which meet the boundary conditions we get the set of low impedance current distribution functions by using EQ107 with $\varphi = 2\pi m/N$ where m is an integer from 1...N/2.

3.5 Numerical methods

The analytical description of the Birdcage derived in the previous sections, provides a basic understanding of how the resonator works. However all the derivations are made with the assumption of symmetry i.e. all components have the same values and the leg and ring spacings are equal. The numerical tools described in this chapter simulate a Birdcage numerically. This allows a verification of the previous analytical derived results and provides some insight of the non symmetric case. A particular example of a low pass Bird-

cage which will be shown and will be constructed later (chapter 3.4). We use two numerical methods to compute resonant frequencies and current distribution for this example. The element values have been chosen to yield approximate resonance frequencies in the range of 10-100MHz.

3.5.1. PSpice computation

The first numerical tool is a electrical analysis program called PSpice. The input of this software package is a list with all the elements used, combined with an instruction set of how to connect them. Further, the experiment to be performed on the circuit and the format of the result have to be defined.

As a first step, Birdcage has to be designed. This is illustrated in Fig.23

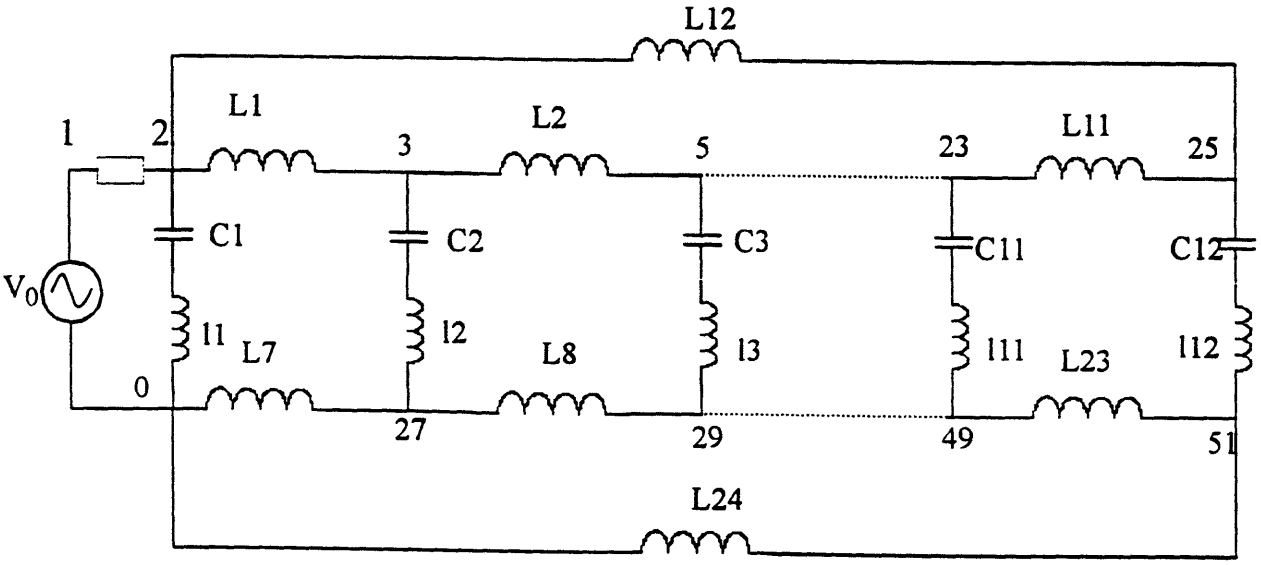

Fig.23: LC network with node labels for Spice analysis

Note that every node is labeled with a number that is used to instruct PSpice how to connect the elements. This example is a 12 leg Birdcage. Appendix B shows the script to perform a frequency response analysis. As a first experiment the leg inductors have been set to zero. The program has problems with

pure imaginary numbers near the resonance frequencies since the currents and voltages approach infinity. Adding small resistors in series with the reactive elements solved this problem.

The voltage source is connected via a resistor to the first leg. For the high impedance resonant modes, the voltage at node 2 should approach the value of the voltage source (i.e. V_0) and for the low impedance modes the voltage at node 2 should be zero. The next figure shows the frequency response at node 2 for a low pass Birdcage with $Z_L = -j/\omega C$,C=55pF and $Z_R = j\omega L$, L=68nH.

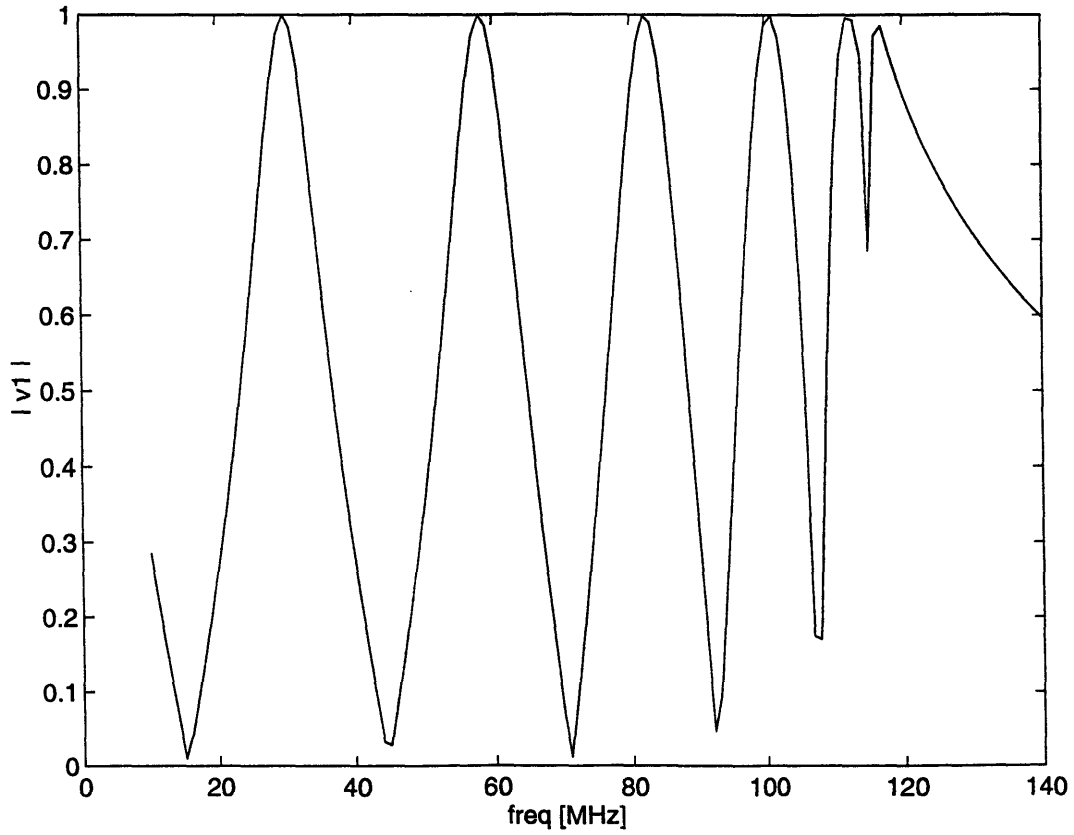

Fig.24: Spice frequency rersponse

Using the same terminology as in the analytical derivation, we can say that the zero points correspond to the series resonant modes and the points where the node 2 voltage approaches 1 correspond to the parallel resonant modes. This is in agreement with the N resonance frequencies derived analytically.

Using the same leg and ring impedances, the resonance frequencies are calculated analytically:

a) high impedance resonant frequencies:

from Appendix A_1 we get the 6 solutions of $J_6(k)$:

Table 5: k solutions for 12 mesh bird cage

k_6	-2.000
k_5	-1.866
k_4	-1.500
k_3	-1.000
k_2	-0.500
k_1	-0.134

Using the simple model discussed in chapter 3.3 where the resonant frequencies are defined as,

EQ108

$$\omega_j = \sqrt{-\frac{k_j}{LC}} \ ,$$

yield,

Table 6: high impedance resonant frequencies for 12mesh Birdcage example

res freq	MHz
ω_6	116.39
ω_5	112.42

Table 6: high impedance resonant frequencies
for 12mesh Birdcage example

ω_4	100.79
ω_3	82.30
ω_2	58.19
ω_1	30.13

These resonance frequencies are equivalent with the frequencies observed with the PSpice frequency plot at the points where the graph approaches 1.0 in Fig.24

b) low impedance resonant modes

Similarly we use the roots (from Appendix A_2) for the low impedance polynomial $J_6(k)$ to compute the second set of resonant frequencies.

Table 7: low impedance resonant frequencies
for 12mesh Birdcage example

ω_6	115.39
ω_5	107.53
ω_4	92.33
ω_3	70.85
ω_2	44.54
ω_1	15.19

These frequencies correspond to the zero points in the PSpice output plot.

The PSpice calculation and the analytical solution for the resonant frequencies yield the same values for a 12 leg low pass Birdcage example as expected.

3.5.2 MATLAB computation

The second method uses the program MATLAB which is a widely used package to perform general numeric calculations. A recursive function performs an impedance calculation as a function of frequency. To see how the algorithm works, let us again consider the Birdcage ladder network where the leg at N/2 is split.

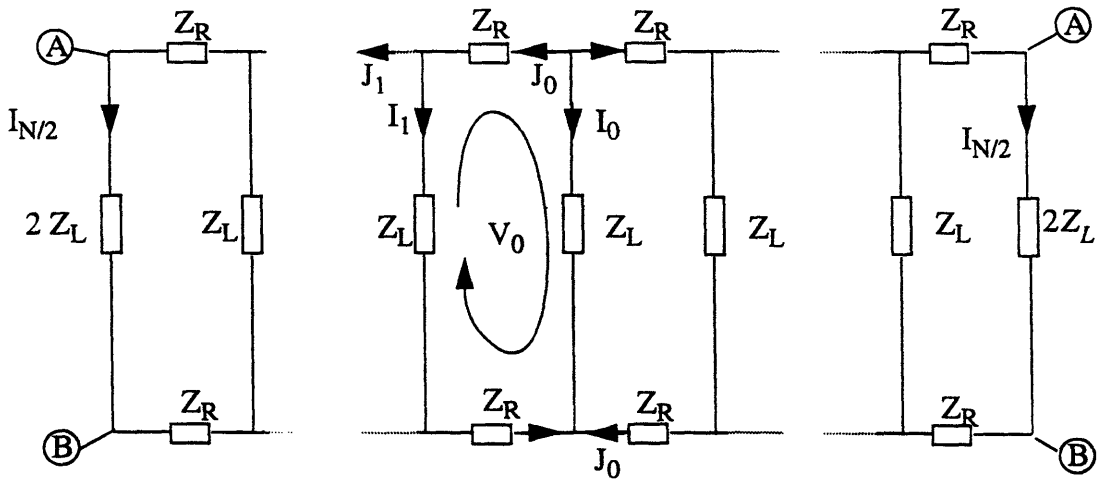

Fig.25: Equivalent circuit for a Birdcage resonator

First consider only one half of the network. Define the impedance at N/2 Z_{init}. Z_{init} has the double value of the leg impedance Z_L due to the splitting of the resonator at position N/2. A MATLAB function, with Z_{init} as input parameter, is called to compute the last mesh i.e. a parallel circuit calculation of $Z_L // (2Z_R + Z_{init})$ to yield a complex impedance Z_{tmp}. Z_{tmp} can now be entered into the same function (i.e. as Z_{init} of a N-1 leg resonator) This recursion is repeated N/2 -1 times. With the last call of the routine (i.e. when N=1) the network has "shrunk" to an equivalent circuit shown in Fig.26.

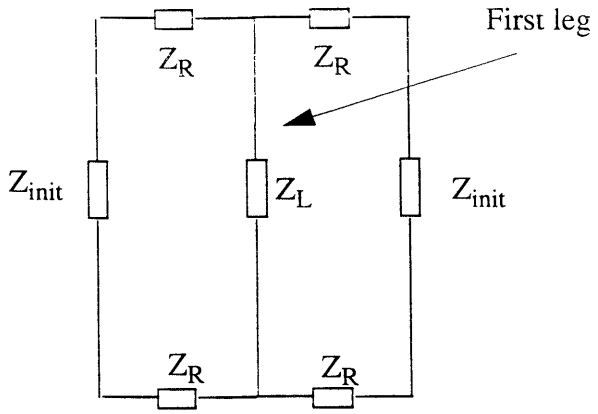

Fig.26: Birdcage compressed with recursive function

The series circuit of Z_{init} and $2Z_R$ yields the total impedance of one side of the resonator without considering Z_L (define $Z'=Z_{init}+2Z_R$). Since we are interested in the impedance of the whole resonator and the left and the right side are identical we conclude that the total impedance without the center Z_L is Z'/2. Therefore the last recursion call computes $Z_L // [\ (2Z_R + Z_{init}) / 2]$ which is the total impedance of the Birdcage resonator.

We can define a frequency vector to compute the total impedance as a function of frequency. Fig.27 shows the frequency response.

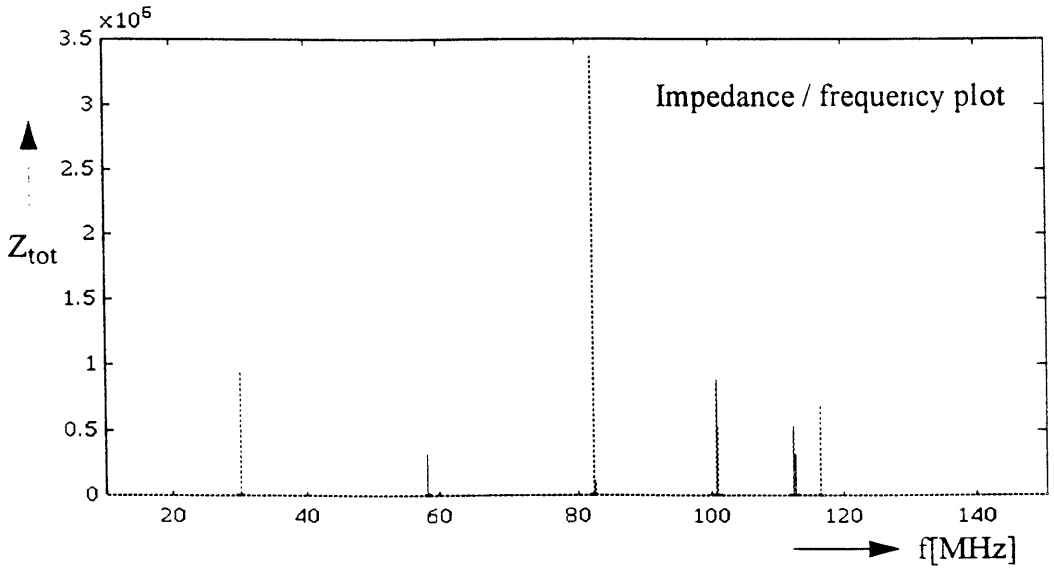

Fig.27: resonance frequencies using the recursive method

Note that the intensities of the peaks vary since a discrete set of frequency points is used to determine the impedances. The impedance values at the high impedance resonance frequencies is infinity, sampling between these points yields the observed variation.

Expanding the y axis of Fig.27 reveals the position of the low impedance resonance frequencies. This is shown in Fig.28.

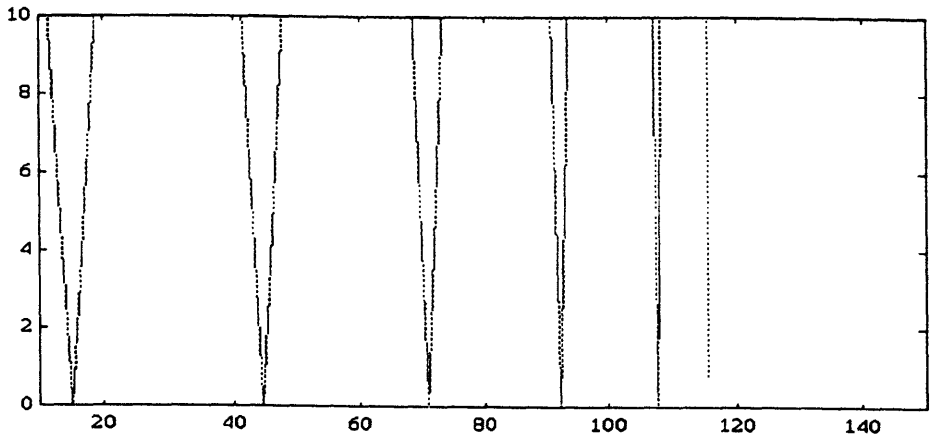

Fig.28: Expansion of Fig.27 to see low impedance resonance frequencies

Note that the position of the peaks and the valleys in Fig.27 and Fig.28 are identical with the resonance frequencies derived analytically and listed in table 6 and table 7.

Fig.29 shows the structure of the recursive function calc_bg.

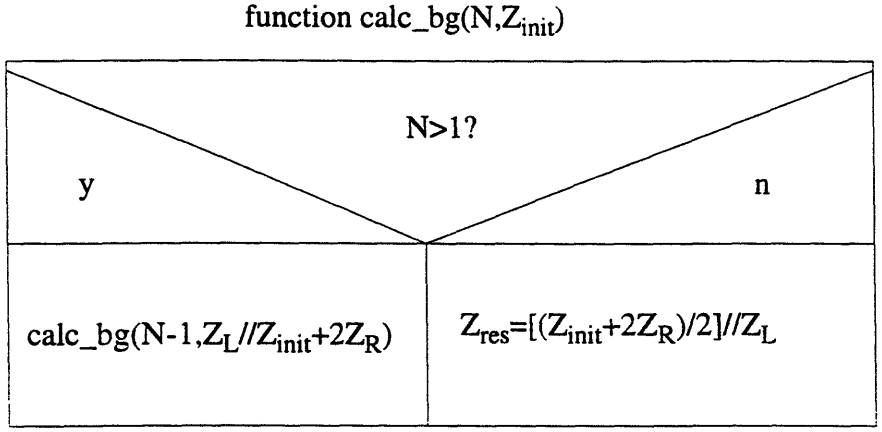

Fig.29: structure of recursive function

In appendix C a listing of the above recursive function can be found.

This recursive numerical method is considerably faster than the approach with the PSpice program for the same number of frequency samples and there is no need to add small resistors.

3.6 RF Field distribution

With the current distributions derived in the last section we can get an idea about the magnetic field generated due to this currents. Using Bio-Savarts law of magnetostatics, (see chapter 3.1) we can superimpose all the individual currents through each of the legs. This has been done numerically with MATLAB. The contribution to the magnetic field by the end rings (i.e. currents through impedances Z_R) has been neglected, since the object to be measured is reasonably far away from the end rings (a couple of cm). Thus the calculation assumes infinitely long wires, carrying currents according to the expressions derived in section 3.4. Since N different resonant frequencies and current distributions are possible, N distinguishable RF field distributions can be obtained with a Birdcage resonator.

The implementation of this numerical calculation can be found in appendix D. The RF field is a vector. A convenient way to easily read the vector field is with arrows which lengths represent the magnitude of the field at the points where they appear on the plot.

The next three figures show potentially useful field maps which can be used to perform NMR experiments. These maps are computed for a 12 leg resonator. The diameter of the circles seen on the plots represent the strength of the current through the corresponding legs.

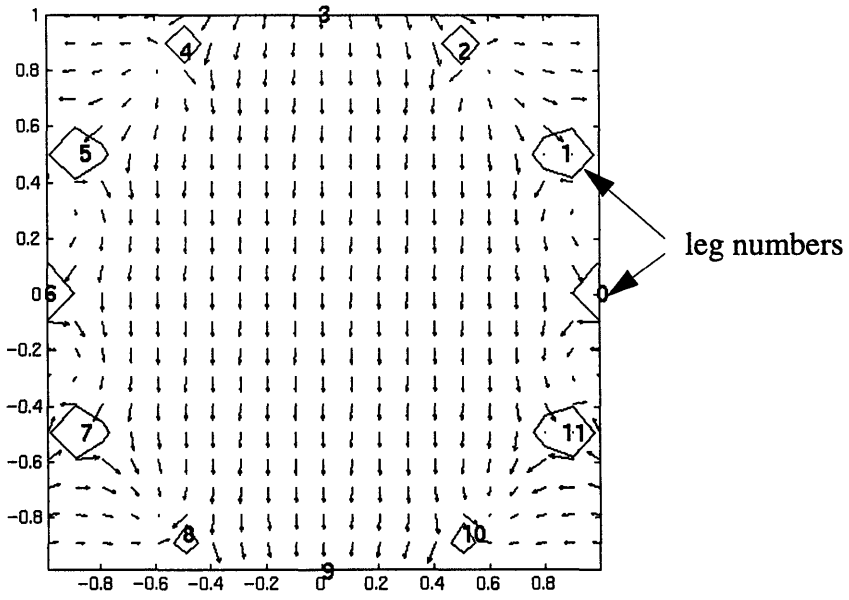

Fig.30: first (homogeneous) mode, high impedance

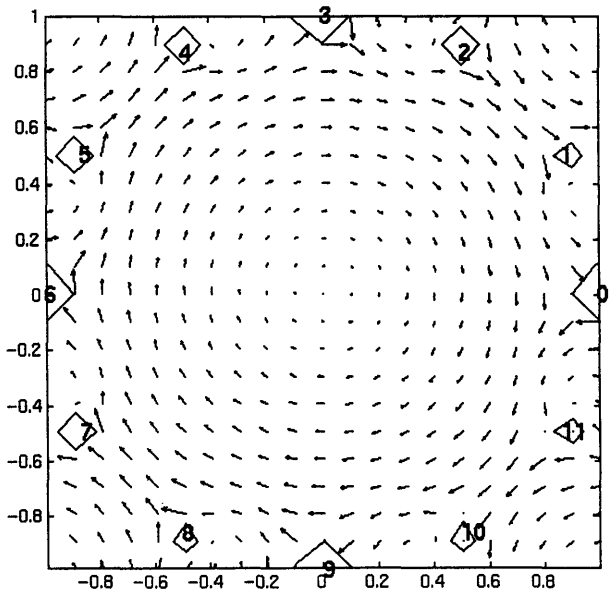

Fig.31: second(gradient) mode, high impedance

l

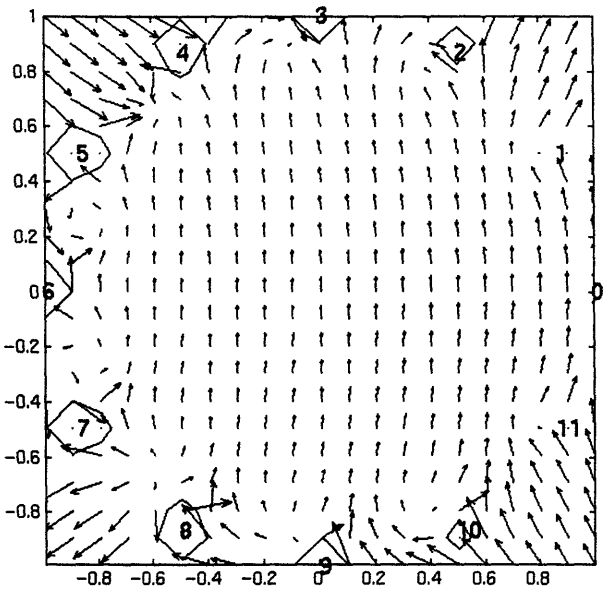

Fig.32: first mode, low impedance

Notice that for the low impedance first mode in Fig.32 the currents through the legs on the right hand side are small. Therefore these legs could be removed. This type of design might be useful for MR application where the organ to be imaged cannot be accessed with a traditional closed loop Birdcage (heart, breast etc.)

3.6.1 Analytical description of the RF field distribution

An analytical way of describing the RF-field inside the resonator can be done by assuming an infinite number of legs. Thus in this limit, the current distribution becomes a continuous function. The current density in the z direction (i.e. direction of the legs) can be written as,

EQ109

$$\vec{J}(\vec{r}) = I_0 \frac{\delta(r-R)}{R} \cos(m\varphi)\hat{z} \ ,$$

where R is the radius of the resonator m the mode and $\vec{r}$ the position vector in cylindrical coordinates.The delta function restricts the current flow to a cylinder in z direction (extending from $-\infty ... +\infty$) and m is the mode.

The Maxwell equations (in vacuum) for magnetostatics are

EQ110

$$\nabla \times \vec{B} = \frac{4\pi}{c}\vec{J} \ ,$$

$$\nabla \bullet \vec{B} = 0 \ .$$

From vector calculus we know that $\nabla \bullet (\nabla \times \vec{A}) = 0$ and thus $\vec{B} = (\nabla \times \vec{A})$. $\vec{A}$ represents any vector field and is called the vector potential. Substituting $\vec{B}$ in EQ110a yields:

EQ111

$$\nabla \times (\nabla \times \vec{A}) = \nabla(\nabla \bullet \vec{A}) - \nabla^2 \vec{A} = \frac{4\pi}{c}\vec{J} \ .$$

There are many choices of $\vec{A}$ which yield the same magnetic vector $\vec{B}$ A valid solution for $\vec{B}$ can be found if we chose $\vec{A}$ to be divergence free. ([7] chapt.5). EQ111 then changes to:

EQ112

$$\nabla^2 \vec{A} = -\frac{4\pi}{c}\vec{J} \ ,$$

which is the Poisson equation with the solution:

EQ113

$$\vec{A}(\vec{r}) = \frac{1}{c}\int_V \frac{\vec{J}(\vec{r}')}{|\vec{r}-\vec{r}'|}d\vec{r}'$$

Note that the x and y components of vector $\vec{J}(\vec{r}')$ are 0 since the current flows along the legs. Therefore the vector potential $\vec{A}(\vec{r})$ has only a z component. Carrying out the integration and taking the curl of $\vec{A}(\vec{r})$ yields magnetic induction vector $\vec{B}$ inside the resonator (r<R):

EQ114

$$\vec{B}(\vec{r}) = \frac{-\mu_0 I_0 r^{n-1}}{2 R^n}(\sin[(n-1)\varphi]\hat{x} + \cos[(n-1)\varphi]\hat{y}) \quad .$$

For n=1 $\vec{B}(\vec{r})$ is constant and thus a homogeneous field distribution results.

For n=2 we get:

EQ115

$$\vec{B}(\vec{r}) = \frac{-\mu_0 I_0}{2}\frac{r}{R^2}[\hat{x}\sin(\varphi) + \hat{y}\cos(\varphi)] \quad .$$

The magnitude in this case increases linearly with the radius, independent of the angle φ . This property can be seen clearly in Fig.31 for the 12 leg Birdcage. This type of resonator can be compared with a 'wrap around' surface coil since the field has a non uniform shape similar to a surface coil.

The possible advantages of this coil design (gradient Birdcage) is subject of the next chapter.

3.7 SNR considerations for Birdcage resonators

In the previous chapter an expression for the magnetic induction inside a Birdcage resonator has been derived from the position of the wires and a continues current distribution. This magnetic field has a time dependency in the form of a complex exponential, i.e. $e^{-j\omega_m t}$ where m is the mode the resonator is tuned to.

The main losses of the coil come from eddy currents generated in the conductive sample (i.e. the human body part) inside the resonator.[8] The time varying B field will induce these eddy currents and thus dissipates power. To see this, we consider the third Maxwell equation,

EQ116

$$\nabla \times \vec{E} = \frac{\partial}{\partial t}\vec{B} \ .$$

Considering the sinusoidal nature of the B field, the term on the right side of EQ116 is then $j\omega\vec{B}$. Furthermore, a conductive media placed in an electric field causes a current to flow. Current density $\vec{J}$ and electric field are related by $\vec{J} = \sigma\vec{E}$, where σ is a proportional constant called the conductivity. Thus EQ116 can be rewritten as

EQ117

$$\nabla \times \vec{J} = j\omega\sigma\vec{B} \ .$$

The power dissipation in a differential volume dV in the tissue is,

EQ118

$$dP = \frac{1}{2\sigma}|\vec{J}|^2 dV \ .$$

This power relation is useful since the noise power received by the MR scanner is proportional to the total power dissipated in the conductive sample and therefore is a measure of the noise. Note that a small fraction of the noise is generated by the resistance of the coil which is assumed to be small compared to the noise power generated by the sample [8].

First we express the power dissipation in a sample placed in a homogeneous Birdcage resonator. The B field is constant and can be written as $\hat{y}B_1$. Writing out EQ117 yields

EQ119

$$\nabla \times \vec{J} = \begin{vmatrix} \hat{x} & \hat{y} & \hat{z} \\ \frac{\partial}{\partial x} & \frac{\partial}{\partial y} & \frac{\partial}{\partial z} \\ J_x & J_y & J_z \end{vmatrix} = \hat{y} j\omega\sigma B_1 \ .$$

Since the B field has only a y component, we get the current density

EQ120

$$\vec{J} = \frac{j\omega\sigma}{2}(z\hat{x} - x\hat{z})B_1 \ .$$

For the power calculation of EQ118 the magnitude square of the current density is needed. A spherical ball is used to model the sample. Therefore it is advisable to write the position vector of $|\vec{J}|^2$ in spherical coordinates,

EQ121

$$|\vec{J}|^2 = \frac{\omega^2\sigma^2}{4}B_1 r^2(\cos^2\theta + \sin^2\theta\cos^2\varphi) \ .$$

Using EQ118 and integrating over the volume of the ball yields

EQ122

$$P_{hm} = \frac{\omega^2 \sigma B_1^2}{8} \cdot \int_0^{a} \int_0^{\pi} \int_0^{2\pi} r^4 \left(\cos^2\theta + \sin^2\theta\cos^2\varphi\right) \sin\theta \, d\varphi \, d\theta \, dr = \frac{a^5 B_1^2 \omega^2 \sigma \pi}{15}$$

where a is the radius of the spherical sample. The result of EQ122 is in agreement with equation 16 in [8].

For the calculation of the power dissipated in the gradient Birdcage, The same method is used. Applying EQ115, i.e. the expression for the B field of the gradient Birdcage, to EQ117 the current density becomes,

EQ123

$$\vec{J} = \frac{j\varpi\sigma B_1}{3R} \left(xz\hat{x} - yz\hat{y} + (y^2 - x^2)\,\hat{z}\right) \quad ,$$

and

EQ124

$$|J|^2 = \frac{\varpi^2 \sigma^2 B_1^2}{9R^2} \cdot r^4 \sin^2\theta \left(\begin{array}{c} \cos^2\varphi\cos^2\theta + \sin^2\varphi\cos^2\theta + \sin^2\theta\sin^4\varphi \\ -2\sin^2\varphi\cos^2\varphi\sin^2\theta + \sin^2\theta\cos^4\varphi \end{array} \right) .$$

Integrating over the volume of the sphere (with EQ118) yields the power dissipated in the ball when placed inside a gradient Birdcage,

EQ125

$$P_{gr} = \frac{4\pi\sigma\omega^2 B_1^2 a^7}{315R^2} \quad ,$$

where B_1 is the magnitude of the RF field at the edge of the coil.

The ratio between the noise power of the gradient and the homogeneous Birdcage at the edge of the sphere (when using a sphere with same radius as the

coil) is

EQ126

$$\frac{P_{gr}}{P_{hm}} = \frac{4}{21}.$$

Since the B field at the edge of the coil is equal (per unit current) for both modes, the signal to noise ratio (SNR) for the gradient Birdcage is $\sqrt{21/4} \approx 2.3$ higher than the homogeneous Birdcage at the edge of the coil. Note that the square root has been taken since the SNR is measured with the voltage noise.

Experimental verification of this hypothesis can be found in chapter 3.8.3.

3.8 Experimental results

So far we derived the characteristics of the Birdcage resonator from theoretical models. In this section we demonstrate that the predictions match "real world" measurements.

3.8.1 Resonance frequencies

We have verified the prediction of the resonance frequencies for a 12 leg low pass Birdcage. An HP 8753 network analyzer was capacitively coupled to one Birdcage leg.

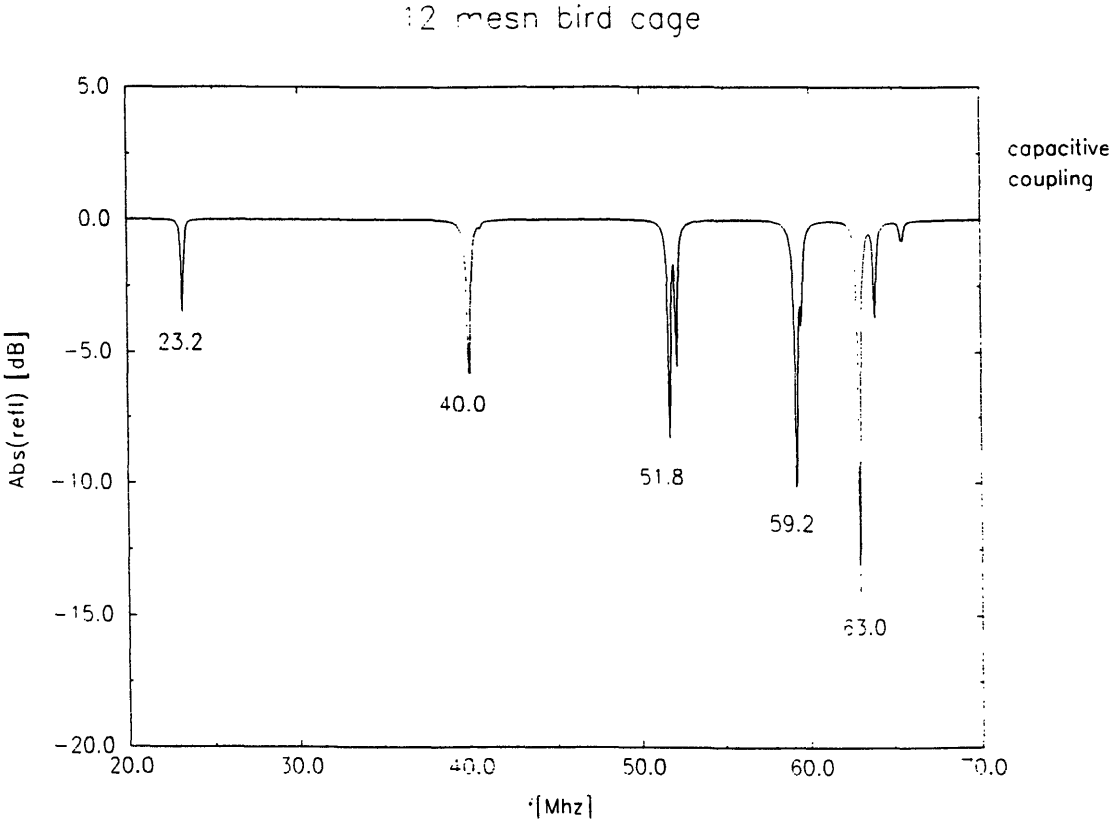

Fig.33: reflection factor of a low pass Birdcage with 55pF leg capacitors

The capacitor values of this resonator have been chosen as 55pF. With the design procedure for low pass Birdcage resonators (see chapter 3) The leg inductors were determined to be 53nH and the ring inductors to be 110nH. The

following table shows a comparison between measured and calculated resonance frequencies:

Table 8: Resonance frequencies [MHz]
with L=110nH; L1=53nH; C=55pF

measured	calculated
23.0	23.0
40.0	41.1
51.8	53.2
59.1	60.4
63.0	64.2
65.4	65.4

The leg capacitors (2*55pF=110pF) have been placed at each end of the legs in order to create as much symmetry as possible. The capacitive coupling to the resonator is illustrated in Fig.34.

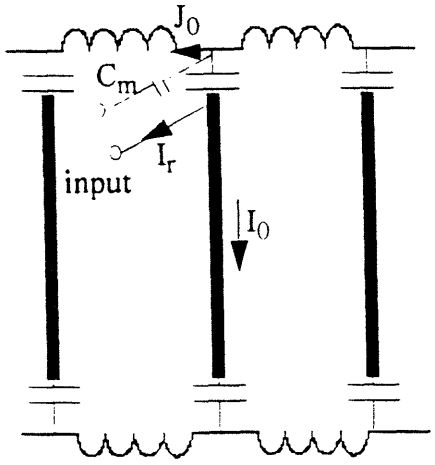

Fig.34: capacitive coupling to the 12 mesh low pass Birdcage

The fat lines in fig.34 represent the legs of the resonator. Note that the end ring inductors are solenoids with 3 turns and 6mm in diameter. In Fig.34 we can see that a current through the matching capacitor C_m is equal to the current returning to the source (I_r), thus the initial condition given in chapter 3 (i.e. $J_0=-I_0/2$) is the same as in above figure. Note that this coupling scheme does not allow a tuning to the low impedance modes, since zero current in the first leg is not possible.

3.8.2 Current distribution

A one turn pick up coil has been placed perpendicular to the legs of the resonator which are constructed from copper shims 15cm long and 1cm in breadth. Fig.35 illustrates the setup for the current measurement.

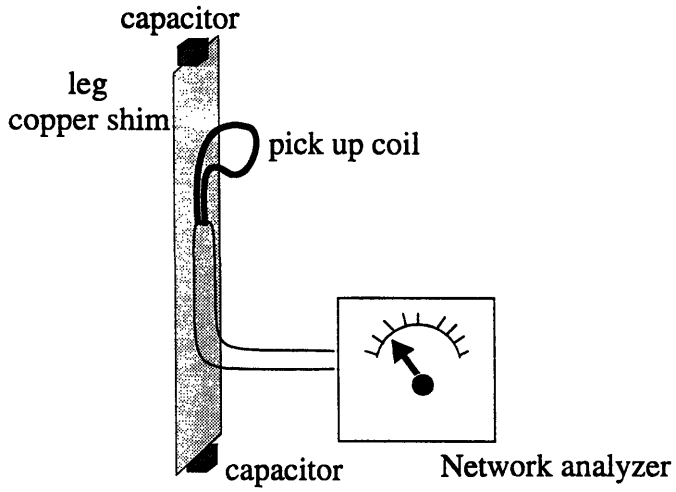

Fig.35: Current measurement at the Birdcage legs

The network analyzer measures both magnitude and phase of the signal picked up by the wire loop. Thus it is possible to distinguish between 'negative' and 'positive' currents. Fig.36 and Fig.38 show the currents measured at the first and second resonant mode.

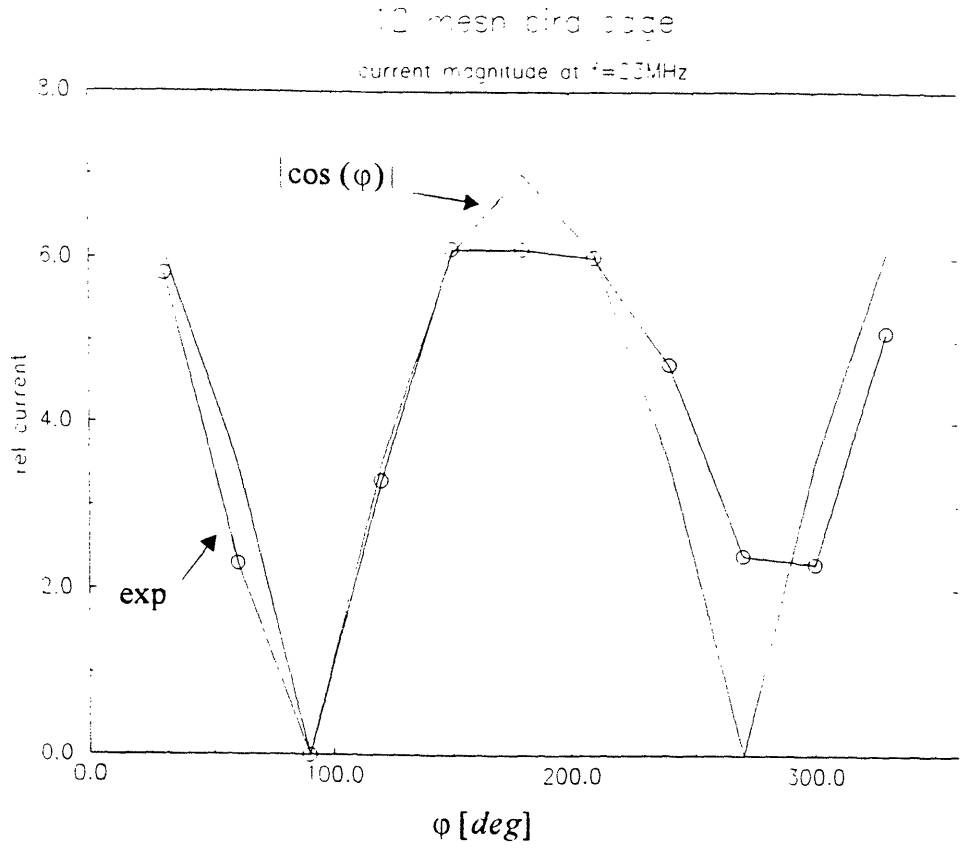

Fig.36: current magnitude measurement with mode = 1

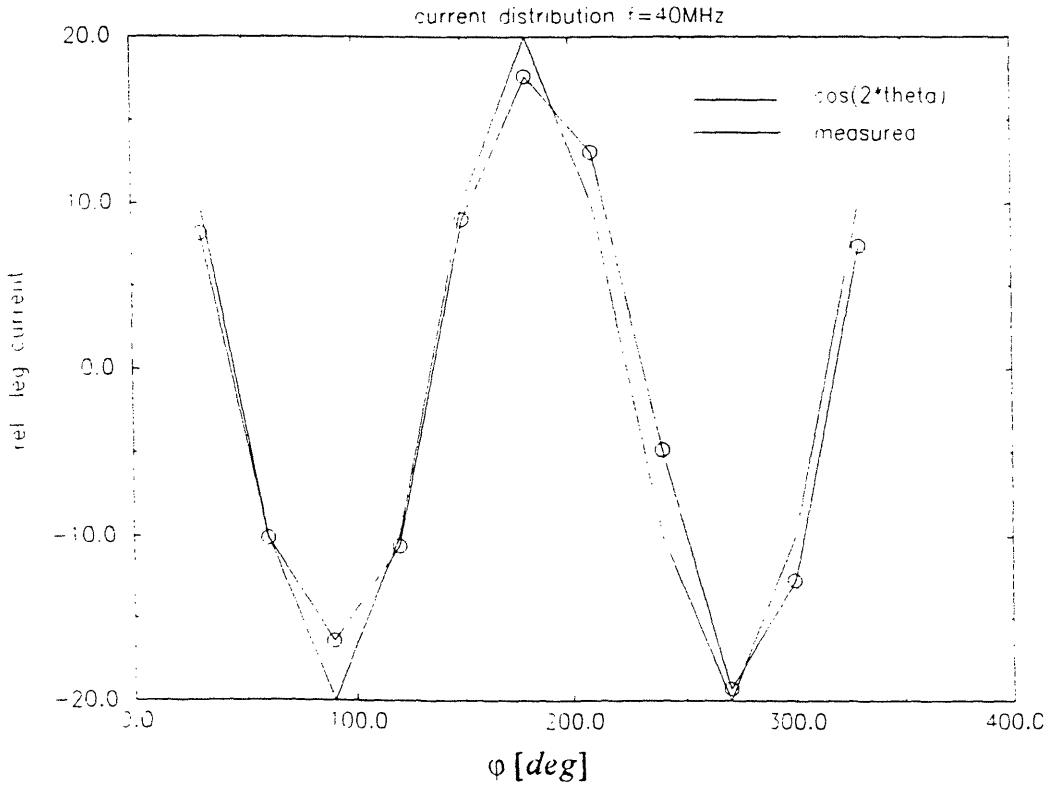

Fig.37: current magnitude measurement with mode = 2

The current distribution determination is a powerful way to get an idea about the symmetry of the Birdcage and to determine whether the resonator is properly functioning. Imagine the case of a broken leg capacitor (or a completely wrong value of a capacitor), the resonator might still be tunable to the required frequency but the NMR images would be of poor quality. A measurement of the current distribution could locate the source of the problem. In chapter 4 we show an improved method of measuring the symmetry of the resonator with a rotating wire loop, that has the advantage of performing a measurement of all the currents at the same time and thus can be used to adjust the Birdcage 'on line'.

3.8.3 Power dissipation

In chapter 3.7 we derived the power dissipation in a spherical sample and predicted that the SNR value of the gradient mode is approx 2.3 times higher than the homogeneous mode. Now we want to verify the expression for the power dissipation experimentally.

We can model the power losses as a parallel resistance to an inductor L_n and then see the frequencies ω_n as resonant frequencies of an equivalent parallel tank circuit. A small part of the power is dissipated in the resistive part (copper shims, non ideal capacitors) of the resonator itself. Fig.38 shows the equivalent circuit.

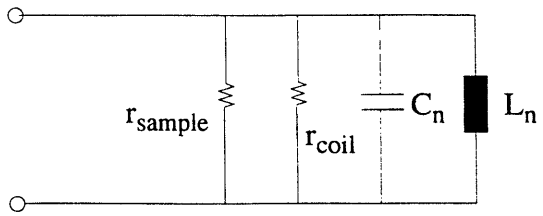

Fig.38: equivalent circuit for mode n

First we estimate r_{coil} and L_n by measuring the Q values (which is defined as the ratio $r_{par}/\omega L$) with known external resistors parallel to the coil. The first Q measurement is done without an external resistor, the second measurement is done with the external resistor r_{ext}. The two obtained Q values (O_1,Q_2) can be used to calculate r_{coil}. With

EQ127

$$Q_1 = \frac{r_{coil}}{\omega_n L_n} ,$$

EQ128

$$Q_2 = \frac{r_{coil} \cdot r_{ext}}{(r_{coil} + r_{ext})\, \omega_n L_n} ,$$

we solve EQ127 for L_n and the substitution it into EQ128 yields:

EQ129

$$r_{coil} = \left(\frac{Q_1}{Q_2} - 1 \right) r_{ext} .$$

Rewriting the parallel circuit of r_{coil} and L_n yields an equivalent series circuit of rs_{coil} and L_n. (i.e. splitting the equation for a parallel circuit in real and imaginary part and assuming that Q >>1)

The results are summarized in the table below in table 9.

Table 9:
measurement of effective inductance and resistor
on the 12 mesh Birdcage tuned to different modes

mode	freq[MHz]	r_{coil}[Ω]	rs_{coil}[Ω]	L_n[nH]
1	23.0	3600	0.5	300
2	40.0	2100	0.29	97
4	59.2	1900	0.09	35

Now we load the coil with a spherical ball filled with saline solution with different amounts of salt. The change in the value of the equivalent series resistor as a function of the saline concentration is due to the power dissipated in the sample. With the knowledge of L_n and the measured Q values, we can determine the total equivalent series resistance rs_{coil} for each mode as a function of the saline concentration

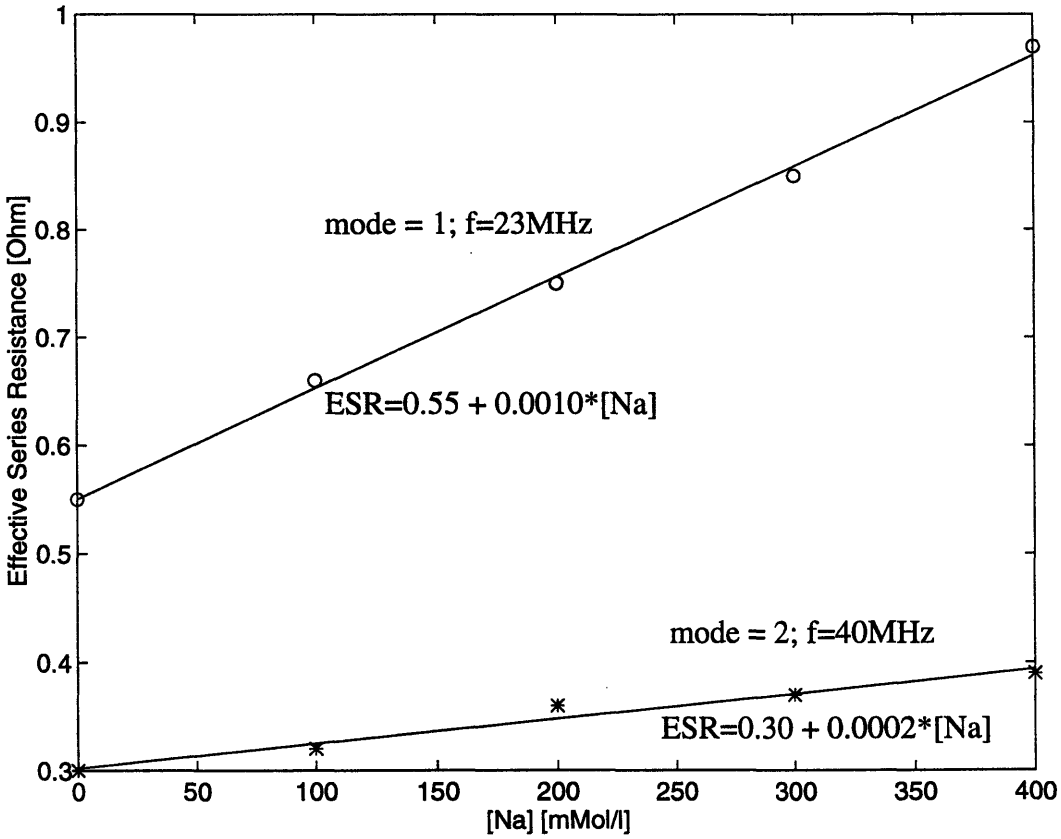

Fig.39:
Effective resistance as a function of sample loading for mode 1 and mode 2 measured with the 12 mesh Birdcage

We can clearly see that a sample with no salt added has the same equivalent series resistance as the resonator with no load at all. This is further evidence that the major loss mechanism is in fact the generation of eddy currents in the conductive solution. Since the B field and the power dissipation were calcu-

lated per unit current, the ratio of the dissipated power values for the two different modes is proportional to the ratio of the equivalent series resistors. Thus the slopes of the curves in the figure above (i.e. dR/dNa) are proportional to the power dissipated in the spherical sample. Considering the actual radius of the sphere (i.e. a=4.9cm), the radius of the resonator (i.e. R=7.2cm) and the two different resonant frequencies (i.e. 23MHz and 40MHz), the theoretical prediction (using EQ122 and EQ125) is

EQ130

$$\frac{rs_{gr}}{rs_{hm}} = \frac{P_{gr}}{P_{hm}} = \frac{4}{21}\left(\frac{a}{R}\right)^2\left(\frac{\omega_2}{\omega_1}\right)^2 = 0.26 \quad .$$

The ratio of the slopes in Fig.39 is 0.22, which agrees well with the theoretical prediction of EQ130.

Furthermore a 16 mesh Birdcage with R=12.7cm has been constructed and an MR experiment was performed. With a spherical sample ($a/R = 0.6$) we predict a SNR increase of approx. 2.3 for the gradient resonator compared with a similar homogeneous resonator.

For the experiment, both resonators (i.e. a GE head coil and our 16 mesh gradient resonator) were driven in quadrature. The measured ratio of the SNR at the edge of the sphere was approx. 2.0.

3.8.4. RF field distribution / transmit, receive fields in the gradient mode

An NMR experiment performed with the 16 mesh resonator has been used to demonstrate the radial RF field distribution. We have collected a series of images (using a spherical sample) with varying values of the RF transmitter power. At each individual pixel of the image, the maximum signal intensity

(as a function of the power) received at a particular power value, corresponds to a $\pi/2$ flip angle of the spin magnetization (see chapter 1). Fig.40 shows the image with the gradient resonator at some medium transmit power level (TG=50). It serves as a location aide for Fig.41

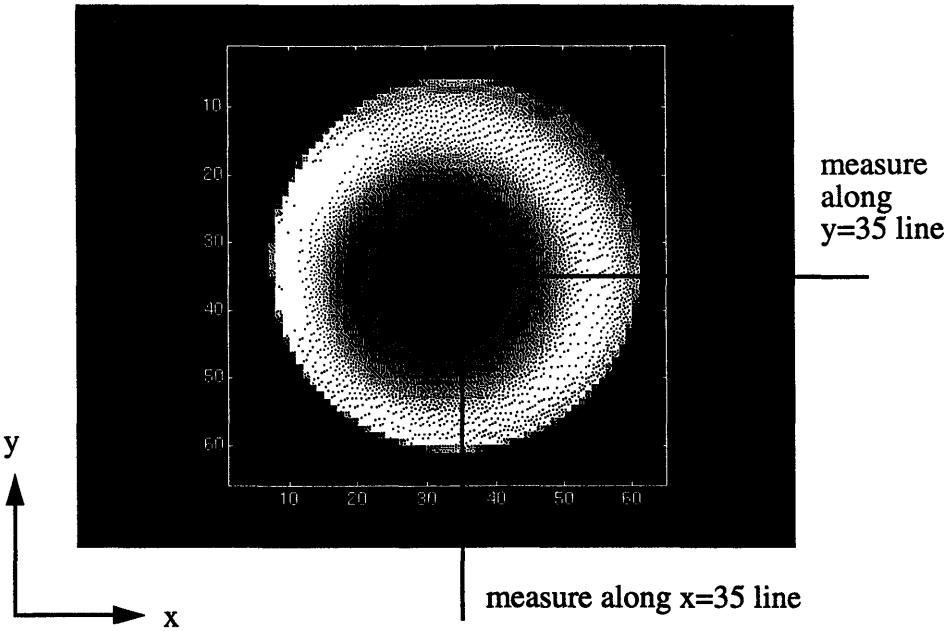

Fig.40: location aide for Fig.41

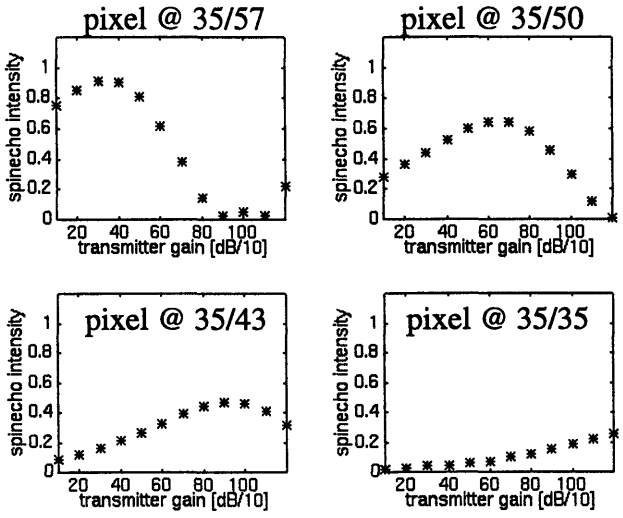

Fig.41: Measure along x=35 line

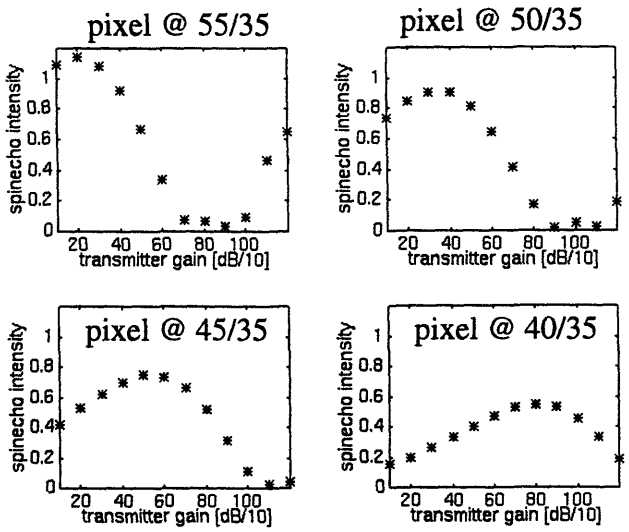

Fig.42: Measure along y=35 line

Clearly, as we go towards the center of the resonator, the intensities of the received signal decreases and the power for a $\pi/2$ flip angle increases.

We now compare the transmit field (i.e. the field to flip the magnetization) and the receive field (i.e. the field received form the flipped magnetization).

The value of the transmit power at the position of the maximum received signal is a measure of the transmit field, and the intensity value at that position is a measure of the receive field. Analyzing the collected data in this way yields the following images

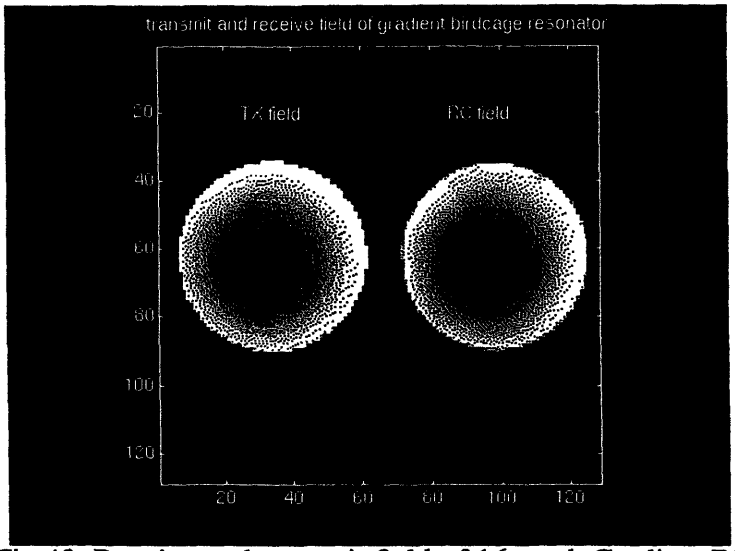

Fig.43: Receive and transmit field of 16 mesh Gradient Birdcage

Note that the resolution of the transmit field is rather low since only 13 different power levels (TG=0..120) have been used in the experiment. Taking a couple of slices at different rows and overlay (after normalization) the receive and transmit field intensities yields the field maps shown in Fig.44. The intensity of the cut through the center of the coil (i.e. at the horizontal line at approx. 65) should decease linearly towards the center, which is clearly the case when we look at the next figures. Note that a cut off for the calculations of the transmit and receive field had to be introduced since the field near the center of the coil is to weak to determine the $\pi/2$ pulse.

Furthermore with the comparison of the transmit and receive field (next figures), we have experimentally verified the principle of reciprocity[6].

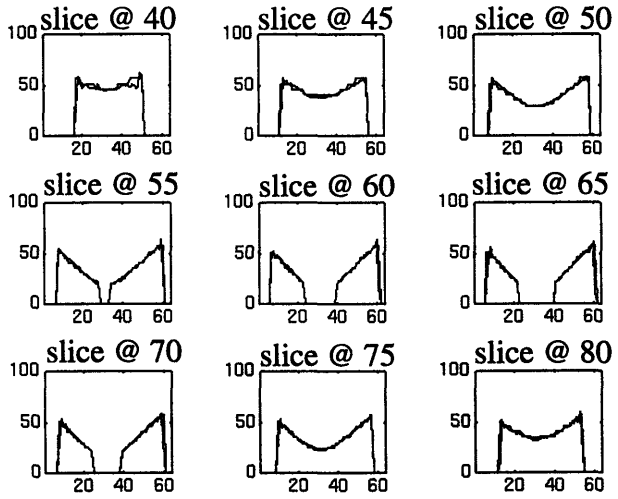

Fig.44: overlaid receive and transmit fields
(low resolution is transmit field)

All calculations and plots have been made on MATLAB. The scripts are shown in Appendix E

4. Practical considerations

4.1 Adjustment of the Birdcage resonator

4.1.1 Motivation

The N/2 resonance frequencies, derived in the previous sections, rely on the fact that the leg and ring impedances (Z_L,Z_R) are precisely matched. In practice however this assumption holds only to a certain degree. In order to make the Birdcage resonator tunable, variable components have to be introduced. It is obvious, that the calibration of a birdcage resonator is rather tedious, since N variable components, and thus N degrees of freedom, have to be adjusted. Even if non symmetries exist, it is still possible to tune and match the resonator to a desired frequency. In other words, there is no way of telling whether the resonator is out of symmetry by just looking at one resonance line. To a certain point, the splitting of the resonance lines can give some indication of the degree of non-symmetry. In practice however, splitting of the resonance lines always occurs and, therefore, is not a reliable check of the symmetry of the Birdcage. This is the motivation for the development of a method that samples the actual currents in all legs.

4.1.2 Measurement of leg currents with wire loop

From Biot Savart law, the magnitude of the magnetic vector field caused by the current through a straight wire, i.e. the resonator leg, decreases with 1/r. Let the straight wire be positioned along the Z axis. Then the direction of the magnetic vector is in the X-Y plane as depicted in Fig.45

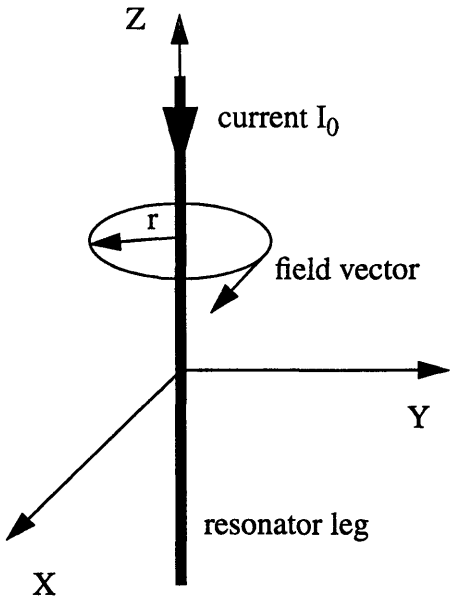

Fig.45: B field due to I_0

Placing a small wire loop so that its enclosed area is perpendicular to the field vector and applying Faradays induction law i.e:

EQ 131

$$\varepsilon = \frac{d}{dt}\Phi(t) \quad ,$$

where $\Phi(t)$ is the magnetic flux caused by current I_0 results in the induced voltage ε. Solving the Biot-Savart law for this case yields,

EQ 132

$$\Phi(t) = \frac{I_0 \mu_0}{r} S \quad ,$$

where r is the radial distance of the small wire loop to the wire with current I_0, S is the surface enclosed by the wire and placed perpendicular to the field lines. (see Fig.35)

Applying a sinusoidal voltage at the input of the Birdcage, (i.e.

$I_0 \sin(\omega_n t)$)that oscillates with the n'th resonance frequency, will result in leg currents with magnitude according to EQ102 or EQ107.

Solving EQ131 for this sinusoidal case yields

EQ 133

$$\varepsilon_i = \frac{d}{dt}\Phi(t) = \frac{I_0 \omega_n \mu_0 S}{r} \cos(\omega_n t) \cos(ni\varphi),$$

where $\varphi = 2\pi/N$ is the angular spacing between the legs, and i the leg number. We can see that the magnitude of the leg current is proportional to induced EMF ε_i, which can be measured with a vector voltmeter. Repeating this procedure for all Birdcage legs yields the current distribution which is a measure of the symmetry of the resonator. Ideally this would match EQ102 or EQ107. Additionally the number of periods represent the mode the Birdcage is tuned to. Fig.36 and Fig.37 show current distributions for two different resonance frequencies. Note that Fig.36 shows the magnitude of the picked up EMF, whereas in Fig.37 the phase information has been used to determine the sign of the current. We can clearly see that the two frequencies represent two modes, namely 1 and 2.

Practically the method is rather inconvenient to adjust the resonator since there is no immediate feedback when the variable components of the birdcage are changed.

It might be feasible to measure the currents with N wire loops (1 loop for each leg) simultaneously and then sample and display the induced voltages with a computer. This would provide "real time" information of the current magnitudes and therefore an on-line adjustment would be possible. However, the hardware requirement of such a device does not justify a follow up on this idea.

4.1.3 Current measurement with rotational loop

A somewhat less "expensive" way of implementing the above procedure in an "on line" manner, could be done with a rotating wire loop connected to an oscilloscope. The practical difficulty here is the connection to the wire loop, which has to be flexible. We could however use a closed loop as "voltage" generator and use its induced voltage to disturb the resonator which then is a measure of the current strength. Again consider a leg of the resonator with a perpendicular placed closed wire loop as depicted in Fig.46

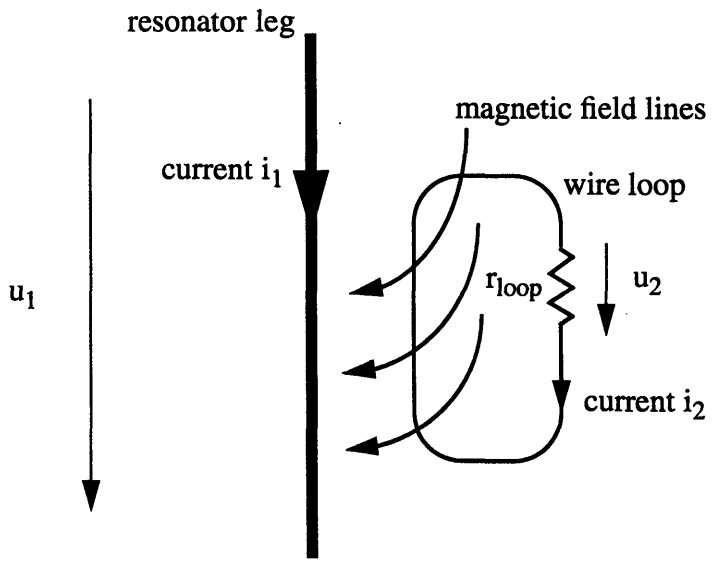

Fig.46: closed wire loop near the Birdcage leg perturbs resonator

Clearly, if the closed wire loop is near the resonator leg, magnetic flux lines, caused by current i_1, cross the enclosed area of the loop and thus introducing coupling between the leg inductor and the loop inductor. Considering this coupling, the relations between currents and voltages are:

EQ 134

$$u1 = -L_1\frac{di_1}{dt} + M\frac{di_2}{dt} \quad ,$$

EQ 135

$$u2 = -L_2\frac{di_2}{dt} + M\frac{di_1}{dt} \quad ,$$

where L_1 and L_2 represent the self inductances of the resonator leg and the wire loop and M the mutual inductance.

EQ 136

$$M = k\sqrt{L_1 L_2} \quad ,$$

where k is the coupling factor i.e. the amount of coupling between the two coils with k=0 for no coupling and k=1 for full coupling. Clearly k is a function of the position of the wire loop. One way of solving EQ134 and EQ135 is to use the Laplace Transform which is defined as:

EQ 137

$$F(s) = \int_{-\infty}^{\infty} f(t)\, e^{-st} \quad .$$

Assuming initial rest condition of the system and using derivative rule of the Laplace Transform EQ134 and EQ135 can be transferred to the s-pace.

EQ 138

$$u_1 = -L_1 i_1 s + M i_2 s \quad ,$$

and

EQ 139

$$u_2 = -L_2 i_2 s + M i_1 s \quad .$$

The resistor r_{loop} represents the small resistance of the closed wire loop. Applying Ohm's law:

EQ 140

$$u_2 = i_2 r_{loop} \quad ,$$

and substituting EQ139 into EQ 140yields

EQ 141

$$i_2 = \frac{Mi_1 s}{(r_{loop} + L_2 s)} \quad .$$

Substituting EQ141 into EQ138 gives

EQ 142

$$\frac{u_1}{i_1} = -L_1 s + \frac{M^2 s^2}{(r_{loop} + L_2 s)} \quad .$$

using EQ140 and r_{loop} -->0, (which is a reasonable assumption since the magnitude of the complex number $L_2 s$ in the denominator of EQ142 is much greater at the operating frequency i.e. 10-200MHz than r_{loop}) yields

EQ 143

$$\frac{u_1}{i_1} = (k^2 - 1) L_1 s = Z_L(k) .$$

The factor u_1/i_1 is the leg impedance in presence of a closed wire loop which couples with coupling factor k to the leg inductance. Since we are operating the Birdcage at a frequency ω_n and assume the magnitude of the input voltage to be constant we can replace the complex variable s with $j\omega_n$. Thus we can write the leg impedance:

EQ 144

$$Z_L(k) = j\omega_{res} L_1 (k^2 - 1) \quad .$$

The coupling k reduces the self inductance of the leg inductor and if the closed wire loop is removed (i.e. k=0) we are left with the impedance due to the self inductance.

Let us consider an optimally adjusted Birdcage that is tuned and matched to the desired frequency ω_n and connected to a voltage generator. Clearly the resonator absorbs all the energy from the voltage source and, thus, there is no power reflected from the resonator. Changing one of the components of the Birdcage will result in a slightly mismatched circuit and thus a small part of the energy will be reflected. In the above discussion we introduced an impedance change by simply bringing the closed wire loop near the leg of the Birdcage. Therefore, intensity of the reflected power is a function of the position of the wire loop.

To illustrate this, let's consider a coil with inductance L and a small resistor R to model the coil losses, to be operated at the frequency ω_{res}. We use the following circuit to match the coil.

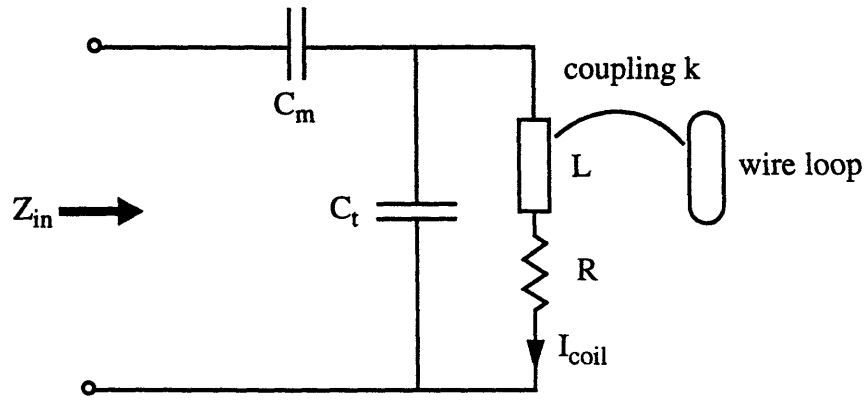

Fig.47: Matched circuit perturbed by a wire loop

If we assume no coupling between the wire loop and the inductance L, we can choose the values of C_m and C_t according to EQ50 in chapter 2.3. Then the circuit is matched and all energy absorbed by resistor R (neglecting losses in C_m and C_t). The reflection factor at the input port can be expressed as

EQ 145

$$\Gamma(k) = \frac{Z_{in} - Z_0}{Z_{in} + Z_0} \quad ,$$

where Z_0 is the characteristic impedance of the transmission line and

EQ 146

$$Z_{in}(k) = -j\frac{1}{\omega_{res}C_m} + \frac{R + j\omega L(k)}{1 - \omega_{res}^2 L(k)\, C_t + j\omega_{res} C_t R} \quad .$$

EQ144 shows the relationship between the coupling k and the inductance L. The reflection factor is a measure of the power reflected from the circuit. In particular it can be written as

EQ 147

$$|\Gamma| = \sqrt{\frac{P_{refl}}{P_{in}}} \quad ,$$

where P_{in} is the power approaching the circuit. The reflected power can be measured easily with a reflection bridge. To illustrate this let $\omega_{res}=10^8$rad sec^{-1}, C_t=95.5pF, C_m=4.5pF, R=0.1Ohm and L=1uH. With these values the circuit of Fig.47 with k=0 is matched. For simplicity it is assumed that the distance from the closed wire loop to the coil is proportional to the coupling constant k i.e.

$$k = c(a - |x|) \qquad \text{for } -a<x<a \quad ,$$

where a is the distance for which k can be assumed to be negligeable and ac the greatest coupling i.e. when the wire loop is closest to the coil at x=0.

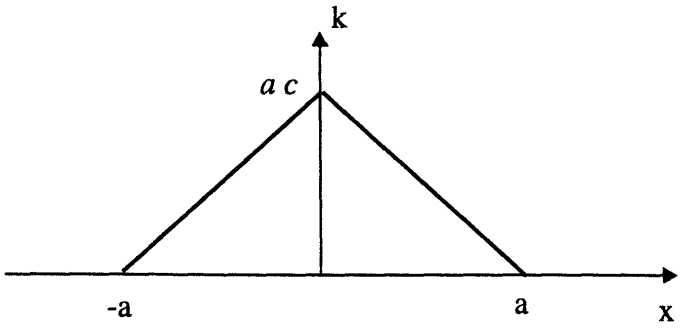

Fig.48
coupling constant k as a function of distance to inductor

Fig.49 shows the complex reflection coefficient as a function of distance x with a set arbitrarily to 10 and c=1/1000

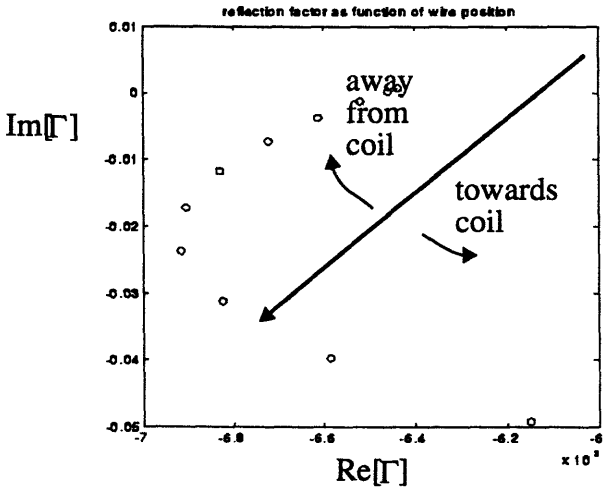

Fig.49: Locus of Γ as a function of wire loop distance

The arrow in above Fig.49 originates at the zero point of the complex reflection plane. As seen from EQ.147 the magnitude of the reflection coefficient is a measure of the reflected power assuming constant input power. Fig.50 shows the magnitude vs. distance.

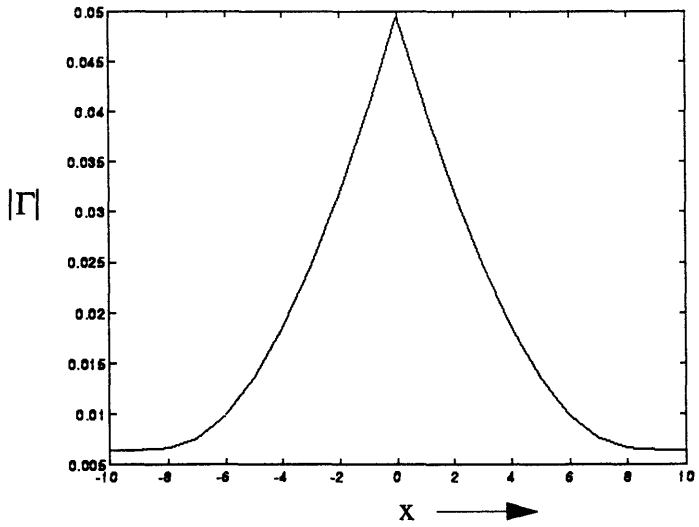

Fig.50: |Γ| as a function of wire loop distance

With the above example, it is clear that the reflection factor is a function of the position of the closed wire loop.

Now we show that the power reflected is a measure of the current I_{coil} (see Fig.47). The power dissipated in R in Fig.47 is

EQ 148

$$P_{dis} = I_{coil}^2 \cdot R = P_{in} - P_{refl} \quad ,$$

with EQ147 and EQEQ149 we can write:

EQ 149

$$P_{refl} = \frac{|\Gamma|^2 I_{coil}^2 \cdot R}{|\Gamma|^2 - 1} \quad .$$

If we assume Γ to be constant (i.e. the wire loop is at a fixed position) then the reflected power is a measure of the current.

In a Birdcage resonator, there are N "coils" (the legs) which carry different currents. Changing one of the inductors yields a similar result as discussed

above for the one coil setup.

To see this, let us consider a Birdcage resonator which is coupled to a voltage source at the first leg and we measure no reflection (i.e. the resonator is matched). Now we perturb the neighbor leg at the right with the closed wire loop. Some reflection on the first leg (where the voltage source is connected) is measured. By placing the wire loop near the left neighbor leg there is exactly the same amount of reflection (symmetry of Birdcage). By placing the wire loop at a leg with no current there is no perturbation and therefore no reflected power. By placing the wire loop near a leg with a high current flow, the perturbation is greater and therefore more reflection is observed. By rotating a closed wire loop inside the resonator with a constant frequency ω_{rot}, the leg position is transformed into time. Thus picking up the reflection as a function of time, allows to measure the N different leg currents. The reflected power can be measured with an oscilloscope and a reflection bridge. Synchronizing the start of the electron beam of the scope with the rotation of the wire loop, yields a standing picture of the current distribution in the Birdcage resonator's legs.

Fig.51 shows the setup from a top view.

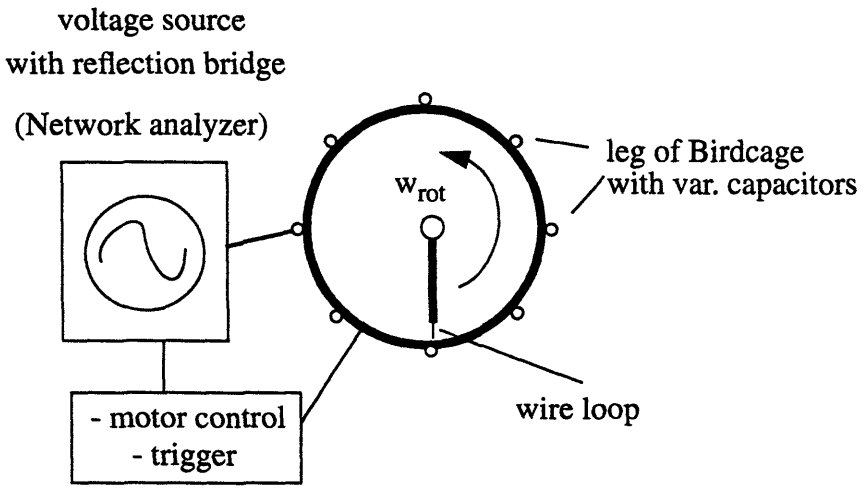

Fig.51: leg current measurement setup

Fig.52. and Fig.53 show current distribution plots for a 16 leg resonator driven in the first and second mode. We can clearly see the difference in the current distribution and the sinusoidal nature of the peak intensities.

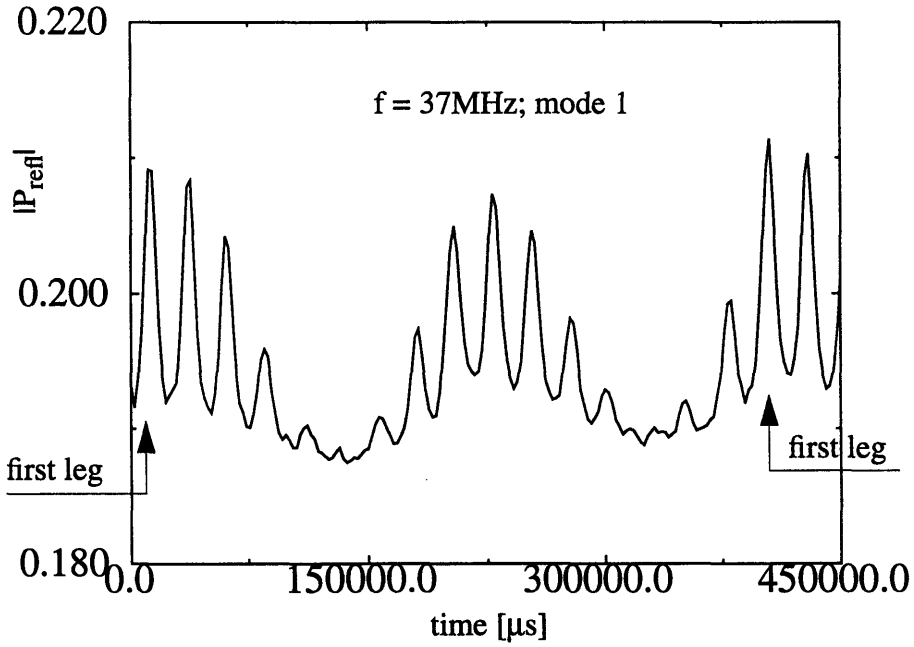

Fig.52:
reflected power measured with an oscilloscope and a reflection bridge

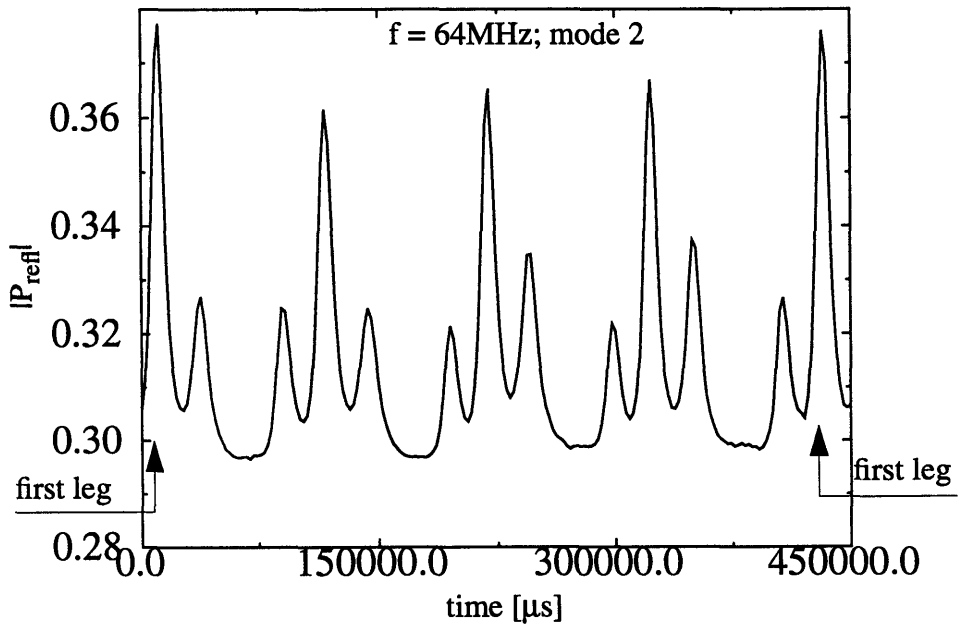

Fig.53: reflected power measured with oscilloscope and reflection bridge

The intensity difference of the reflected power measurements in Fig.52 and Fig.53 can be explained when considering EQ133. The resonance frequency for the homogeneous mode on this 16 leg resonator is 37MHz and for the gradient mode 64MHz. Thus we expect a 64/37=1.73 increase in induced voltage in the wire loop for the gradient coil. Since we measure the power reflection, we expect an intensity difference between the two modes of $1.73^2 \approx 3$ which agrees fairly well with above plots.

This setup has proven to be a useful tool in adjusting the Birdcage resonator and to trouble shoot broken resonators since it gives direct evidence of the amount of current carried in each leg.

4.1.3.1 Circuit description of motor and trigger control board

Appendix F shows the circuit diagram of the electronic board which controls the motor used for the rotation of the wire loop and the trigger pulses used to start a reflection measurement. A stepper motor has been used since it can be controlled easily. Each step is an angular increment of 7.5deg. The motor has 2 stator coils which have to be energized alternatively. Assume that on each coil a DC voltage (i.e. V_1 and V_2) is applied. One step involves the change of the polarity V_1 while V_2 stays at the same value. The next step is performed by changing the polarity of V_2 while V_1 is kept and so forth. 48 such steps equals a full rotation of the rotor.

IC_3 (inverted schmitt trigger) combined with R_1,R_2 and C_1 form the master oscillator of the circuit. There is not much stability requirement on the rotation, thus this simple oscillator is appropriate. IC_1,IC_3 and IC_5 perform the timing explained above. The RC high pass filters (R_3,C_2, R_5,C_3) are used to eliminate the DC offset oft the output voltages of IC_1 pin9 and IC_1 pin 5. The

motor driver circuit is made out of IC_2,T_1,T_2 and IC_4,T_3,T_4. IC_6 and IC_7 are dividers to provide a trigger pulse to the Network analyzer at each full cycle of the motor (division by 48).

5. References

1. Harold Elford Johns, The physics of Radiology, 4th edition, Published by Charles C. Thomas

2. Cecil E. Hayes , William A. Edelstein, John F. Schenk, Ottward M. Mueller and Matthew Eash, Journal of Magnetic Resonance 63, 622-628 (1985)

3. James Troop, Journal of Magnetic Resonance 82,51-62 (1989)

4. Thomas C. Farrar, Introduction to NMR Spectroscopy, The Farrragut Press, Chicago

5. Charles P. Slichter, Principles of Magnetic Resonance, 3rd edition Springer-Verlag NewYork Berlin Heidelberg

6. D.I. Hoult, R.E. Richards, J. of Magnetic Resonance 24,71 (1976)

7. J.D.Jackson, Classical Electrodynamics, 2nd edition, Published by John Wiley&Sons, Inc.

8. D.I. Houldt, P.C. Lauterbur, J. of Magnetic Resonance 34, 425 (1979)

9. H.R. Schwarz, Numerische Mathematik, Teubner-Verlag, Stuttgart Germany 1988

10. M.D. Harpen, Magnetic Resonance in Medicine, 29:263-268 (1993)

11. David K. Cheng, Engineering Electromagnetics Addison-Wesley 1993

6. Conclusions

The conclusions to be drawn from this thesis are:

1) a polynomial approach can be used to predict the resonance frequencies of a Birdcage
2) there are a total of N (number of legs) resonance frequencies in a Birdcage resonator i.e. N/2 at high impedance and N/2 at low impedance.
3) the Signal to Noise Ratio (SNR) at the edge of the Birdcage when tuned to the second mode is approx. a factor of two higher than the SNR when tuned to the first mode
4) the symmetry of a Birdcage can be measured "on the bench" with a rotating wire loop.

7. Final remarks / acknowledgments

This Birdcage resonator project started out of the desire to have an RF coil with an increased Signal to Noise Ratio and with a field of view which covers the whole cortex of the brain (see chapter 1). We have shown that the gradient Birdcage has these characteristics and could be used for MR experiments which require an enhanced Signal to Noise Ratio. (functional MR imaging)

Several tools have been developed in order to construct and understand the Birdcage resonator. Further the adjustment of the coil turned out to be quite a task, which lead to the development of the current measurement tool described in chapter 4. Considering all these little sideways, the project was more than just a construction of an MR coil.

I would like to thank my supervisor Robert Weisskoff for the freedom he gave me to go my own ways, David Cory for the stimulating discussions and Jerry Ackerman for his offer to supervise this work for the EE department.

Cambridge, May 11. 1995

Appendix A

Determination of Birdcage polynomial coefficients

A.1 Determination for high impedance modes

The ring and leg currents of the Birdcage resonator can be expressed with EQ63 in chapter 3.3. Substitution of $k = Z_R/Z_L$ into EQ 63 yields

EQ150

$$I_{n+1} = I_n - 2J_n k \ ,$$

and

EQ151

$$J_{n+1} = J_n - I_{n+1} \ .$$

With the initial conditions for the unperturbed Birdcage (i.e. I_0, J_0=-1/2I_0) we can generate all consecutive current values with EQ150 and EQ151. To do that we create 2 tables. The first table contains the leg currents I_n and the second table the ring currents J_n. As we start the recursion we can see that polynomials $I_n(k)$ and $J_n(k)$ are generated. In order to apply an easy scheme to compute the coefficients we define:

EQ152

$$I_n = I_0 \sum_{i=0}^{n} c_{n,i} \cdot k^i$$

EQ153

$$J_n = -\frac{I_0}{2} \sum_{i=0}^{n} d_{n,i} \cdot k^i$$

A coefficient table, with the row entries being the exponent i and the column entries being the leg number n, can be generated. With the definition of EQ152 and EQ153 the coefficients can be computed in a simple way. The multiplica-

tion of $-2J_n$ with k in EQ152 can be seen as shifting the entries in the J_n table one position to the right. Therefore the n+1 row in the I_n table can be computed by shifting row n of the J_n table one position to the right and adding row n of the I_n table. Similarly with EQ151, the n+1 row in the J_n table is computed by adding twice the value of the n+1 row of the I_n table to the n row of the J_n table.

With the polynomial coefficients for I_n being $c_{n,i}$ and for J_n being $d_{n,i}$ (as in EQ152 and EQ153) the recipe can be written in a more compact form:

to get c_{n+1} row:shift d_n row one to the right and add the c_n row.

to get d_{n+1} row: add double values of c_{n+1} row to d_n row.

The following tables show the implementation of the procedure the first 8 polynomials

Table 10: $c_{n,i}$

n \ i	0	1	2	3	4	5	6	7
0	1	0	0	0	0	0	0	0
1	1	1	0	0	0	0	0	0
2	1	4	2	0	0	0	0	0
3	1	9	12	4	0	0	0	0
4	1	16	40	32	8	0	0	0
5	1	25	100	140	80	16	0	0
6	1	36	210	448	432	192	32	0
7	1	49	392	1176	1680	5632	448	64

Table 11: $d_{n,i}$

n \ i	0	1	2	3	4	5	6	7
0	1	0	0	0	0	0	0	0
1	3	2	0	0	0	0	0	0
2	5	10	4	0	0	0	0	0
3	7	28	28	8	0	0	0	0
4	9	60	108	72	16	0	0	0
5	11	110	308	352	176	32	0	0
6	13	182	728	1248	1040	416	64	0
7	15	280	1512	3600	4400	2880	960	128

Note that this coefficients are independent of the physical parameters (i.e. lumped and distributed elements) of the Birdcage. In order to get the ring and leg currents of a N mesh resonator, we consider the polynomials $J_{N/2}$ and $I_{N/2}$. In chapter 3 we had to modify the leg impedance at position N/2 (i.e. $2Z_L$) in order to represent the Birdcage with an open ladder network. Therefore the $J_{N/2}$ and $I_{N/2}$ polynomials have to be modified too. To do that we apply Kirchhoffs law for the N/2 mesh:

EQ154

$$I_{N/2-1}Z_L - 2J_{N/2-1}Z_R - 2I_{N/2}Z_L = 0 \ .$$

Rewriting EQ154 yields:

EQ155

$$I_{N/2} = \frac{1}{2}\left(I_{N/2-1} - 2J_{N/2-1}\frac{Z_R}{Z_L} \right) \ ,$$

and

EQ156

$$J_{N/2} = J_{N/2-1} - I_{N/2} \ .$$

Rewriting EQ155 and EQ156 yields,

EQ157

$$-2J_{N/2} = I_{N/2-1} - 2J_{N/2-1} - 2J_{N/2-1}k \ .$$

a b c d

Term a is the modified ring current, term b is the leg current at position N/2-1, term c is the ring current at position N/2-1 and term d is the ring current at position N/2-1 shifted one position to the right. (multiplication with k) Note that these terms are in the same format as the entries in table 1 and table 2. Therefore the following scheme can be used to compute the modified coefficients for $J_{N/2}$. (i.e. $d_{N/2,i}$):

add $d_{N/2-1}$ row to right shifted $d_{N/2-1}$ row.

add result to $c_{N/2-1}$ row

To get familiar with the procedure, let us consider a 12 mesh Birdcage resonator. From table 2 we can get the coefficients for the ring current $-2J_5$ and add the shifted version as suggested in above rule:

$d_{5,0}$	$d_{5,1}$	$d_{5,2}$	$d_{5,3}$	$d_{5,4}$	$d_{5,5}$	$d_{5,6}$
11	110	308	352	176	32	0
+						
0	11	110	308	352	176	32

Adding the result to the c_5 row(table 1):

0	1	2	3	4	5	6
11	121	418	660	528	208	32
+						
1	25	100	140	80	16	0

results in the polynomial $J_6(k)$:

EQ158

$$J_6(k) = -\frac{I_0}{2}(12 + 146k + 518k^2 + 800k^3 + 608k^4 + 224k^5 + 32k^6) \quad .$$

Now $J_6(k)$ represents the ring current with a $2Z_L$ leg impedance at position N/2.

The boundary condition derived in chapter 3 is:

EQ159

$$J_{N/2} = 0 \quad .$$

Applying EQ159 to EQ158 yields the following solutions for k:

Table 12: k solutions for 12 mesh bird cage
high impedance

k_6	-2.000
k_5	-1.866
k_4	-1.500
k_3	-1.000
k_2	-0.500
k_1	-0.134

A2 Determination for low impedance modes

In a similar manner as for the coefficients for the high impedance case, we can compute the coefficients for the low impedance modes. The only difference is the initial condition which is:

EQ160

$$I_0 = 0 \quad ,$$

and

EQ161

$$J_0 = \frac{1}{2} \ .$$

Using the rules of Appendix A_1 we get:

Table 13: $c_{n,i}$

n \ i	0	1	2	3	4	5	6	7
0	0	0	0	0	0	0	0	0
1	0	1	0	0	0	0	0	0
2	0	2	2	0	0	0	0	0
3	0	3	8	4	0	0	0	0
4	0	4	20	24	8	0	0	0
5	0	5	40	84	64	16	0	0
6	0	6	70	224	288	160	32	0
7	0	7	112	504	960	580	384	64

and

Table 14: $c_{n,i}$

n \ i	0	1	2	3	4	5	6	7
0	1	0	0	0	0	0	0	0
1	1	2	0	0	0	0	0	0
2	1	6	4	0	0	0	0	0
3	1	12	20	8	0	0	0	0
4	1	20	60	56	16	0	0	0
5	1	30	140	224	144	32	0	0
6	1	42	280	672	420	352	64	0
7	1	56	504	1680	2340	1412	832	128

Using the same boundary condition as in A_1 for a 12 leg birdcage example, we get for $J_{N/2}$:

EQ162

$$J_6(k) = 32k^6 + 192k^5 + 432k^4 + 448k^3 + 210k^2 + 36k + 1 = 0 \ .$$

Solving EQ12 yields:

Table 15: k solutions for 12 mesh bird cage
low impedance

k_6	-1.9659
k_5	-1.7071
k_4	-1.2588
k_3	-0.7412
k_2	-0.2929
k_1	-0.0341

Appendix B: PSpice List for 12 Mesh bird cage

```
*12 mesh bird cage resonator
.op
.param ind=68nH
.param cap=55pF
.param capr=0.0000001
.param indr=0.0000001

vin1 2 0 ac 1.0
rl1 2 3 {indr}
rl2 4 5 {indr}
rl3 6 7 {indr}
rl4 8 9 {indr}
rl5 10 11 {indr}
rl6 12 13 {indr}
rl7 14 15 {indr}
rl8 16 32 {indr}
rl9 0 17 {indr}
rl10 18 19 {indr}
rl11 20 21 {indr}
rl12 22 23 {indr}
rl13 24 25 {indr}
rl14 26 27 {indr}
rl15 28 29 {indr}
rl16 30 31 {indr}
rl17 42 43 {indr}
rl18 44 45 {indr}
rl19 46 47 {indr}
rl20 48 49 {indr}
rl21 54 55 {indr}
rl22 56 57 {indr}
rl23 58 59 {indr}
rl24 60 61 {indr}
c1 2 33 {cap}
c2 4 34 {cap}
c3 6 35 {cap}
c4 8 36 {cap}
c5 10 37 {cap}
c6 12 38 {cap}
c7 14 39 {cap}
c8 16 40 {cap}
c9 42 50 {cap}
c10 44 51 {cap}
c11 46 52 {cap}
c12 48 53 {cap}
```

```
l1 3 4 {ind}
l2 5 6 {ind}
l3 7 8 {ind}
l4 9 10 {ind}
l5 11 12 {ind}
l6 13 14 {ind}
l7 15 16 {ind}
l8 32 42 {ind}
l9 17 18 {ind}
l10 19 20 {ind}
l11 21 22 {ind}
l12 23 24 {ind}
l13 25 26 {ind}
l14 27 28 {ind}
l15 29 30 {ind}
l16 31 54 {ind}
l17 43 44 {ind}
l18 45 46 {ind}
l19 47 48 {ind}
l20 49 2 {ind}
l21 55 56 {ind}
l22 57 58 {ind}
l23 59 60 {ind}
l24 61 0 {ind}
rc1 33 0 {capr}
rc2 34 18 {capr}
rc3 35 20 {capr}
rc4 36 22 {capr}
rc5 37 24 {capr}
rc6 38 26 {capr}
rc7 39 28 {capr}
rc8 40 30 {capr}
rc9 50 54 {capr}
rc10 51 56 {capr}
rc11 52 58 {capr}
rc12 53 60 {capr}
;rs 24 0 0.1
;rss 10 2 0.1
.ac lin 500 20.000meg 100.000meg ; *ipsp*
.probe
;.print ac v(2) vp(2)
;.print ac im(c1) ip(c1) im(c2) ip(c2)
;.print ac im(c3) ip(c3) im(c4) ip(c4)
;.print ac im(c5) ip(c5) im(c6) ip(c6)
;.print ac im(c7) ip(c7) im(c8) ip(c8)
;.print ac im(c9) ip(c9) im(c10) ip(c10)
```

```
;.print ac im(c11) ip(c11) im(c12) ip(c12)

;.print ac vr(41) vi(41) ir(r1) ii(r1)
.end
```

Appendix C MATLAB listings for recursive method

a) Main program

```
clear
l=68e-9;
c=55e-12;
w=[1e6*2*pi:1e5:150e6*2*pi];
z=calc_bg(6,l_imp(l,0,w),c_imp(c,0,w),c_imp(c/2,0,w));
axis([10 150 0 10]);
plot(w/2/pi/1e6,abs(z));
```

b) Function for calculating ladder network

```
function zres=calc_bg(n_mesh_half,zr,zl,zinit)
%calculates Birdcage impedances with recurscive model
if (n_mesh_half>1)
 zres=calc_bg(n_mesh_half-1,zr,zl,par(zinit+2*zr,zl));
 else
 zres=par((zinit+2*zr)/2,zl);
end
```

c) Impedance calculation finctions for Capacitors and inductors

```
function y=c_imp(capacity,esr,w)
%calculate complex impedance od capacitor
y=esr-j*(w.*capacity).^(-1);


function y=l_imp(inductance,r,w)
%calculate complex impedance of inductor
y=r+j*w*inductance;
```

c) function for parallel circuit computation

```
function zres=par(zin,zr)
%calculate parallel circuit of two impedances
zres=zr.*zin.*(zin+zr).^(-1);
```

Appendix D MATLAB listings for RF field plot generation

1. script : creation of field with wire position and current values

```
% definition in space
resx=20; %x resolution
resy=20; %y resolution
xmax=1; %max x
ymax=1; %maxy
xmin=-0.99;
ymin=-0.99;

dx=(xmax-xmin)/resx;
dy=(ymax-ymin)/resy;

x=[xmin:dx:xmax];
y=[ymin:dy:ymax];
xind=[1:length(x)];
yind=[1:length(y)];

%definition for currents and positions of wire
mesh=12; %# of meshes
curindex=[1:mesh];
cur=zeros(1,mesh);
phi=pi/4;
%enter ccurrents
cur(1)=0;
cur(2)=sin(phi);
cur(3)=sin(2*phi);
cur(4)=sin(3*phi);
cur(5)=sin(4*phi);
cur(6)=sin(5*phi);
cur(7)=sin(6*phi);
cur(8)=sin(7*phi);
cur(9)=sin(8*phi);
cur(10)=sin(9*phi);
cur(11)=sin(10*phi);
cur(12)=sin(11*phi);

posindex=[1:mesh]; %enter pos. of wire n with

phi=pi/6; %current cur(n)
xpos=zeros(1,mesh);
ypos=zeros(1,mesh);
xpos(1)=1;
ypos(1)=0;
```

```
xpos(2)=cos(phi);
ypos(2)=sin(phi);
xpos(3)=cos(2*phi);
ypos(3)=sin(2*phi);
xpos(4)=cos(3*phi);
ypos(4)=sin(3*phi);
xpos(5)=cos(4*phi);
ypos(5)=sin(4*phi);
xpos(6)=cos(5*phi);
ypos(6)=sin(5*phi);
xpos(7)=cos(6*phi);
ypos(7)=sin(6*phi);
xpos(8)=cos(7*phi);
ypos(8)=sin(7*phi);
xpos(9)=cos(8*phi);
ypos(9)=sin(8*phi);
xpos(10)=cos(9*phi);
ypos(10)=sin(9*phi);
xpos(11)=cos(10*phi);
ypos(11)=sin(10*phi);
xpos(12)=cos(11*phi);
ypos(12)=sin(11*phi);

%enter pos. of wire n with
%current cur(n)

%calculation of b vector fields
dummy=zeros(length(x),length(y));
allbx=[]; allby=[];
for n=1:mesh,
 allbx=[allbx dummy];
 allby=[allby dummy];%create array of empty matr
end;

for n=1:mesh,
 ox=xpos(n); oy=ypos(n);
 current=cur(n); % position of wire
 [px,py]=meshdom(x-ox,y-oy);% px = x comp. of position
 % py = y comp. of position
 bx=(px.^2 + py.^2).^(-1) .* current .* py .* (-1);
% x comp of field at x,y
 by=(px.^2 + py.^2).^(-1) .* current .* px; % y comp of field at x,y
 all_ind_beg=((n-1)*length(x))+1; % indicies of field n in all
 all_ind_end=all_ind_beg-1+length(x);
 allbx(1:length(y),all_ind_beg:all_ind_end)=bx;
%put field n into array
```

```
allby(1:length(y),all_ind_beg:all_ind_end)=by;

end
```

2. Display of field and wires

```
% super imposing of individual fields
wire_num=[1 2 3 4 5 6 7 8 9 10 11 12];
show_wire=1; %show wire on plot
bxtot=dummy; %reset field
bytot=dummy;
tresh=10; %treshold for elimination
%clf;
axis([1,length(x),1,length(y)]);
[X,Y]=meshgrid(x,y);  % display axis in square

for i=1:length(wire_num),
 n=wire_num(i);
 all_ind_beg=((n-1)*length(x))+1; % indicies of field n in all
 all_ind_end=all_ind_beg-1+length(x);
 %load and sum
 bxtmp=allbx(1:length(y),all_ind_beg:all_ind_end);
 bytmp=allby(1:length(y),all_ind_beg:all_ind_end);
 if show_wire
 contour(X,Y,sqrt(bxtmp.^2+bytmp.^2),[tresh tresh],'-k');
 hold on
 end;
 bxtot=bxtot+bxtmp;
 bytot=bytot+bytmp;
end;


i=find(sqrt(bxtot.^2+bytot.^2)>tresh); % eliminate infinite
if length(i) ~= 0 % fields if exist

 bxtot(i)=zeros(1,length(i))';
 bytot(i)=zeros(1,length(i))';
end;

quiver(X,Y,bxtot,bytot,1,'-k'); % plot field arrows
hold off;

for i=1:length(wire_num),
 set(text(xpos(i),ypos(i),sprintf('%i',i-1)),'Color',[0 0 0],'FontSize',18);
end
```

```
axis('square');
getax;
```

Appendix E: Scripts for MATLAB to analyze NMR data

E.1: Reading data from GE MR scanner

```
function y = rsigna(fname,dim);
 % A = rsigna(fname,dim)
% reads raw image from signa (with first 80bytes cut)
% and put data into matrix A wit dimensions dim
 fid=fopen(fname,'r'); %open file for reading
if(fid<0)
 error('file open error');
 break;
end
[A count]=fread(fid,'int16'); %read into matrix
 count
if (count~=dim(1)*dim(2))
 error('dimension mismatch');
 break;
end %check dimensions
fclose(fid);

ind=0; %init index for straight matr
B=zeros(dim(1),dim(2));
for j=1:dim(2),
 for i=1:dim(1),
 ind=ind+1;
 B(i,j)=A(ind);
 end
end
y=B; %return matrix
```

function shoot: gets pixel intensity at x,y for num images --> vector

```
function y = shoot(x,y,matr,num,dim)
%usage y=shoot(x,y,matr,num,dim);
%shoots @(x,y) trough num images with size dim contained in matr

b1=matr(x,y:dim(2):y+(num-1)*dim(2));
y=b1;
```

function show90: plot intensities as function of power for 4 locations on image

```
clf; %clear current figure
tg=[0 10 20 30 40 50 60 70 80 90 100 110 120]; %transm gain values
norm=1/1500; %normalization factor
x=[65 65 65 65];
y=[60 55 50 45]; %chose 4 different coord
```

```
for i=1:4,
 subplot(220+i);
 plot(tg,norm*shoot(x(i),y(i),tot,13,[128 64]),'*k'); %plot shot at (x(i),y(i)
 s=sprintf('spin echo intensity @ {%i/%i}',y(i),x(i));
 title(s);
 xlabel('transmitter gain [dB/10]');
 ylabel('spinecho intensity');
 axis([10 120 0 1.2]);
 getax;
end;
```

function get90: finds position of power where max signal

```
function [pow,int] = get90(tg)

%usage [pow int] = get90(tg)
% pow = max power ( 90 position)
% int = intensity at this position
% tg = vector containing power and intensities

[y,pos] = max(tg(2,:)); % pos of maximum intensity
err=0;
if ( pos >= length(tg(2,:)) )
 err=1;
end

if (y<300)
 err=1;
end

pow=0;
int=0;

if (~err)
 pow=10^(tg(1,pos)/200);
 int=tg(2,pos);
end
```

script trans.m: display of transmit and receive field

```
tra=zeros(128,64);
rec=zeros(128,64);
tg=[0 10 20 30 40 50 60 70 80 90 100 110 120];
for k=30:100,
 for l=1:64,
 tmp=shoot(k,l,tot,13,[128 64]);
```

```
 h=[tg;tmp];
 [a,b]=get90(h);
 if (a>0)
 tra(k,l)=1/a;
 rec(k,l)=b;
 end
 end
end
'plotting....'

clf;
tra=tra/max(max(tra))*64;
rec=rec/max(max(rec))*64;
image([tra rec]);
colormap('gray');
axis('square');
title('transmit and receive field of gradient birdcage resonator');
text(25,20,'TX field');
text(85,20,'RC field');

figure(gcf+1);
clf;
slices=[40 45 50 55 60 65 70 75 80];
for k=1:length(slices),
 subplot(330+k);
 plot([1:64],tra(slices(k),:)','k',[1:64],rec(slices(k),:)','k');
 title(sprintf('slice @ %i',slices(k)));
 axis([1 64 0 100]);
 getax;
end
```

Appendix F

Birdcage adjustment tool hardware